Successful Correction of Patient-Derived iPSCs for SCN8A-Related Developmental and Epileptic Encephalopathy Using an advanced CRISPR-Cas9 system

Youn, Song Ee

Department of Medicine
Graduate School
Yonsei University

Successful Correction of Patient-Derived iPSCs for SCN8A-Related Developmental and Epileptic Encephalopathy Using an advanced CRISPR-Cas9 system

Advisor Kang, Hoon-Chul

A Dissertation Submitted

to the Department of Medicine

and the Committee on Graduate School

of Yonsei University in Partial Fulfillment of the

Requirements for the Degree of
Doctor of Philosophy in Medical Science

Youn, Song Ee

June 2025

Successful Correction of Patient-Derived iPSCs for SCN8A-Related Developmental and Epileptic Encephalopathy Using an advanced CRISPR-Cas9 system

This certifies that the Dissertation of Youn, Song Ee is approved

Committee Chair	**Kim, Chul Hoon**
Committee Member	**Kang , Hoon-Chul**
Committee Member	**Kim, Won-Joo Kim**
Committee Member	**Kim, Hyongbum Henry**
Committee Member	**Eun, Baik Lin**

Department of Medicine
Graduate School
Yonsei University
June 2025

ACKNOWLEDGEMENTS

I would like to express my deepest and most sincere gratitude to my esteemed advisor, Professor kang, Hoon-Chul of the Department of Pediatrics, Yonsei University College of Medicine, for his outstanding mentorship, unwavering support, and invaluable guidance throughout the course of my doctoral studies. His profound academic insight and constant encouragement have been instrumental in the successful completion of this dissertation.

I am profoundly grateful to the members of my dissertation committee for their invaluable contributions to this research. My sincere appreciation is extended to Professor kim, Chul-Hoon (Chair) of the Department of Pharmacology, Yonsei University College of Medicine; Professor kim, Won-Joo of the Department of Neurology, Yonsei University College of Medicine; Professor kim, Hyung-Bum of the Department of Pharmacology, Yonsei University College of Medicine; and Professor Eun, Baik Lin of the Department of Pediatrics, Korea University College of Medicine. Their critical reviews, expert advice, and constructive feedback were essential in elevating the quality and expanding the scope of this study.

Furthermore, I would like to express my deepest gratitude to Mr. Jihun Kim, a research scientist, for his invaluable contributions throughout the entire process of neuronal differentiation from iPSCs and pharmacological experiments, as well as for his insightful analysis of the experimental results. I am also deeply grateful to Dr. Zhejiu Quan for establishing patient-derived iPSCs and generating isogenic iPSCs with normal function using advanced genome editing technologies. Their combined efforts not only laid the foundation for this study but will also serve as a cornerstone for future investigations.

This research was supported by the Basic Science Research Program through the National Research Foundation of Korea (NRF) funded by the Ministry of Education (grant number: RS-2025-00555034) and by a grant of Korea Health Technology R&D Project through the Korea Health Industry Development Institute (KHIDI), funded by the Ministry of Health and Welfare, Republic of Korea (grant number: RS-2025-02263053, RS-2024-00405260) and by Korea Drug Development Fund funded by Ministry of Science and ICT, Ministry of Trade, Industry, and Energy, and Ministry of Health and Welfare (grant number: RS-2025-02213662).

Finally, I would like to express my sincere thanks to the professors of the Department of Pediatrics at Kyung Hee University Hospital at Gangdong and Kyung Hee University for their support and advice, which enabled me to expand the scope of my research at their institutions.

TABLE OF CONTENTS

LIST OF FIGURES

LIST OF TABLES

ABSTRACT

Successful Correction of Patient-Derived iPSCs for SCN8A-Related Developmental and Epileptic Encephalopathy Using an advanced CRISPR-Cas9 system

Background:

Mutations in the SCN8A gene are major contributors to developmental and epileptic encephalopathies (DEEs), leading to early-onset seizures and neurodevelopmental impairments. However, effective disease models and therapeutic strategies remain limited.

Objectives:

This study aimed to model SCN8A-related epilepsy using patient-derived induced pluripotent stem cells (iPSCs), perform genetic correction through prime editing, and compare the neurophysiological and pharmacological responses between mutant and corrected neurons.

Methods:

iPSCs were generated from a patient harboring the SCN8A c.4871T>G (p.Ile1624Ser) mutation and genetically corrected using prime editing. Neurons were differentiated by lentiviral expression of the transcription factors ASCL1, DLX2, and NGN2. Neural network activity was assessed using microelectrode array recordings, and the pharmacological effects of phenytoin and lacosamide were evaluated.

Results:

Patient-derived neurons exhibited hyperexcitability, frequent bursting, and hypersynchrony, whereas corrected neurons showed normalized electrophysiological activity. Prime editing effectively restored neural network function. The effects of phenytoin and lacosamide on network burst indices were more pronounced in corrected neurons, suggesting a tendency toward drug resistance in patient-derived neurons. Furthermore, complementary effects of the two drugs were observed, indicating the potential utility of combination therapy.

Conclusion:

The patient-specific iPSC-derived neuron model faithfully recapitulated SCN8A-related epilepsy. Genetic correction normalized pathological neuronal activity, and drug responsiveness was successfully evaluated using patient-derived cells, highlighting the potential of precision genome editing and personalized pharmacological strategies.

Key words: *SCN8A*; induced pluripotent stem cells; prime editing; epilepsy; neuronal hyperexcitability; multielectrode array

1. Introduction

Developmental and epileptic encephalopathies (DEEs) are a group of disorders characterized by severe cognitive and behavioral impairments that exceed what would be expected from seizure activity alone, often occurring in the context of underlying disorders such as cortical malformations. Many of the epileptic syndromes classified as DEEs have a genetic etiology and include monogenic disorders. In these syndromes, the genetic mutation itself may have a direct impact on neurodevelopment, independent of the effects of recurrent seizure activity. Thus, the developmental impairments observed in these genetic disorders may result not only from frequent epileptic activity but also from the intrinsic effects of the gene mutations on neurodevelopment. [Scheffer et al, 2017; Hebbar et al, 2020]. In the context of etiology, a wide range of neurobiological mechanisms and epilepsy-associated genes have been identified. From the perspective of genetically determined epilepsy, the impact of a single gene mutation on disease expression tends to be greater when epilepsy has an early onset, particularly in childhood. These genes are typically characterized by low tolerance to functional disruption, such that even minor variations can lead to significant dysfunction. Consequently, the frequency of pathogenic variants in these genes is inversely correlated with their prevalence in the general population. [Ellis et al, 2020]. Among monogenic epilepsies, channelopathies—disorders caused by defects in specific ion channels—constitute the largest subgroup, with mutations in voltage-gated sodium channels being the most prevalent. Sodium Channel Subunit-Alpha1.1 (Nav1.1), -Alpha1.2 (Nav1.2), and -Alpha1.6 (Nav1.6), encoded by *SCN1A*, *SCN2A*, and *SCN8A*, respectively, are the three major voltage-gated sodium channels expressed in the central nervous system and are commonly implicated in epilepsy when mutated [Trimmer et al, 2004]. In this study, we focused on genes encoding these sodium channels, which represent the most common genetic causes of monogenic

epilepsy. Specifically, we designed our research around *SCN8A*, a gene increasingly recognized for its role in early-onset epileptic encephalopathies. Nav1.6 is predominantly localized at the axon initial segment and nodes of Ranvier, where it plays a critical role in the initiation and propagation of action potentials [Musto et al, 2020; Meisler et al, 2021]. Epilepsy caused by mutations in the *SCN8A* gene was first identified in 2012 and has since been recognized as a cause of a broad spectrum of epileptic disorders, ranging in severity from self-limited epilepsy to severe developmental and epileptic encephalopathies [Sole et al, 2020; Meisler et al. 2016]. Epilepsy-associated *SCN8A* gene mutations are most commonly single amino acid substitutions and are predominantly spontaneous (de novo) in origin [Meisler et al. 2016]. Epilepsy-related mutations in sodium channel genes exhibit cell type–specific functional consequences. In inhibitory neurons (GABAergic neurons), such mutations are typically associated with loss-of-function, leading to reduced inhibitory control. In contrast, in excitatory neurons (glutamatergic neurons), they are more commonly associated with gain-of-function, resulting in increased excitatory drive. Mutations in the *SCN8A* gene can lead to either overactivity or decreased activity of sodium channels, affecting neuron function [Meisler et al. 2016]. Notably, *SCN8A*-related epilepsies are most frequently linked to gain-of-function mutations in glutamatergic neurons, contributing to cortical hyperexcitability and seizure susceptibility.

In functional studies utilizing disease models, animal models such as mice and zebrafish are widely used; however, these models often fail to fully recapitulate human disease phenotypes. While it remains challenging to investigate the influence of environmental factors, there is clear evidence that everyday variables—such as stress, weather, sleep patterns, and exposure to illness—can significantly modulate the clinical expression of genetic epilepsies. Furthermore, it is plausible that systemic environmental exposures, some of which may yet be unidentified, also contribute to disease manifestation and variability in human patients [Ellis et al, 2020]. Based on

the well-established premise that induced pluripotent stem cells (iPSCs) enable the generation of patient-specific isogenic controls, this study was designed to utilize iPSC technology, gene-editing tools, and neurophysiological assays to develop a disease model of *SCN8A*-related epilepsy and to evaluate cellular responses to pharmacological interventions.

2. MATERIALS AND METHODS

2.1 Subjects and Research Design

Our research specifically focused on ion channel genes associated with epilepsy, emphasizing the identification of alterations in Voltage-Gated Sodium Channels. One particular focus was *SCN8A*-associated epilepsy with encephalopathy, a condition characterized by recurring seizures, impaired brain function, and cognitive disabilities.

We performed Next-Generation Sequencing (NGS) on participants who consented to supplementary genetic analysis using previously collected DNA samples. Library construction was carried out using a highly sensitive and precise protocol developed by the Department of Diagnostic Laboratories, and sequencing was focused on detecting pathogenic variants in critical ion channel genes, including *SCN8A*. Bioinformatic tools were utilized to validate the mutations and correlate them with the patients' clinical phenotypes. we selected a patient with SCN8A-related epileptic encephalopathy with de novo variant. (Table 1).

Furthermore, I derived iPSCs from blood samples of the patient harboring *SCN8A* mutation, following the parents of the patient consent. These iPSCs were differentiated into neuronal cells to establish an *in vitro* disease model for *SCN8A*-related epilepsy. Using this platform, I evaluated the efficacy of two pharmacological agents with distinct mechanisms of action to determine their potential as personalized therapies for this condition.

Table 1. *SCN8A* patient information

Title	Information
Screening Number	8AKSW
Sex	Male
Gene Mutation	*SCN8A*
ACMG Classification	Likely pathogenic
Accession	NM_014191.3

Nucleotide	c.4871T>G (exon 28)
Amino Acid	p.lle1624Ser (Voltage sensing domain IV, S4)
Zygosity	Heterozygosity
Inheritance pattern	De novo
Diagnosis	Epilepsy with myoclonic atonic seizures
Birth history	Intrauterine pregnancy 40weeks, 3.22kg, Normal spontaneous vaginal delivery
Seizure onset	7-month-old
Seizure status	Drug-resistance
Developmental status	(18-month-old) cognition 14 months*, language 19 months*, social function >9 months*, motor 13 months*, SQ 100 (6-year-10-month-old) FSIQ 53, SQ 46.7
Brain MRI	Suggesting previous germinal matrix hemorrhage, right caudothalamic groove

*a developmental age equivalent
FSIQ, Full Scale Intelligence Quotient; SQ, Social Quotient

2.2 Next Generation Sequencing (NGS) - Procedures for performing NGS, including library preparation, sequencing platform details, and bioinformatics pipeline for variant identification and annotation.

Genomic DNA (gDNA) samples were obtained from patients through the Department of Diagnostic Laboratory Medicine and sequenced using either the NextSeq 550Dx system or the NovaSeq 6000 instrument (Illumina, San Diego, California, United States). Libraries for sequencing were constructed using a DNA enrichment protocol designed to maximize sensitivity and precision in variant detection (Figure 1).

This sequencing method has been validated in previous studies, ensuring reliable detection of pathogenic mutations. As part of a preliminary study, I conducted targeted gene panel sequencing in 278 children diagnosed with developmental and epileptic encephalopathy (DEE). A customized gene panel was employed, including genes associated with DEE, to investigate the clinical implications of genotype-phenotype correlations. The analysis involved a comprehensive review of clinical characteristics, including treatment efficacy stratified by genotype.

Through this approach, I identified patients harboring *SCN8A* mutations and hypothesized that sodium channel blockers could be an effective treatment option for these individuals. This insight laid the foundation for exploring tailored therapeutic strategies for *SCN8A*-related epilepsy.

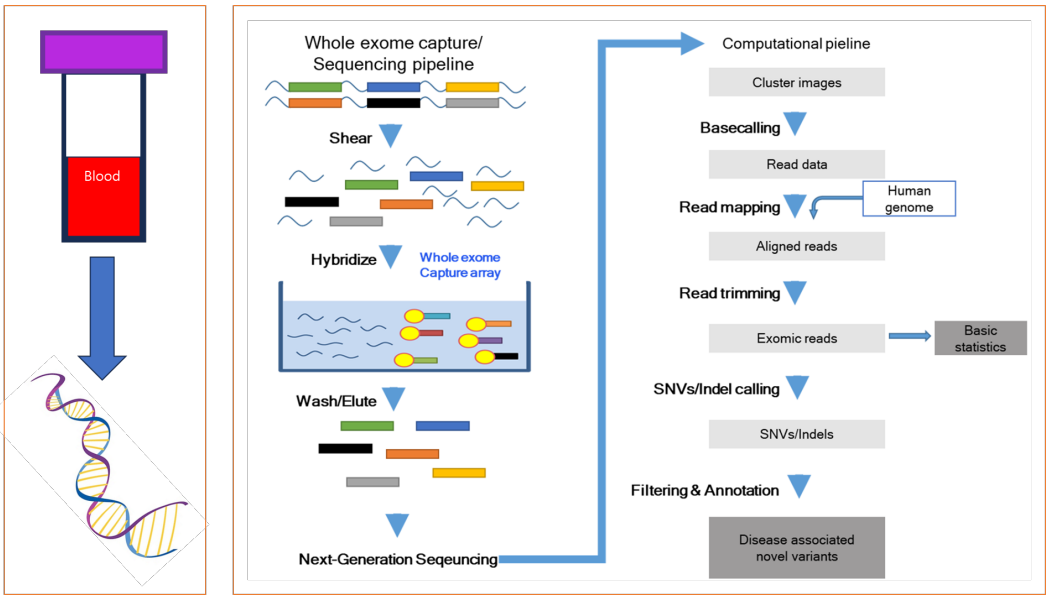

Figure 1. illustrates the workflow of NGS used to identify genetic variants in patients. The process begins with DNA extraction, followed by sequencing using a Whole Exome Sequencing approach. This method, combined with a previously established gene panel for epilepsy, enabled the detection of genetic variants in patients suspected to have SCN8A-related conditions.

2.3 Genome DNA Extraction from Blood - Extraction of genomic DNA from blood samples using validated protocols and kits, ensuring high purity and integrity for downstream applications.

gDNA was isolated from the nuclei of White Blood Cells (WBCs) derived from patient

blood samples using the FavorPrep™ Blood / Cultured Cell Genomic DNA Extraction Mini Kit (Favorgen, Ping Tung, Taiwan), which includes Proteinase K and is compatible with various downstream applications. The extraction process was performed according to the manufacturer's protocol, with additional steps to ensure higher purity.

Blood Collection and Handling : Up to 6 ml of whole blood was collected from each patient into an EDTA tube to prevent clotting. The blood was mixed gently by inverting the tube to ensure even anticoagulant distribution. While immediate processing was preferred, the samples were stored at 4°C for a maximum of 3 days when immediate extraction was not feasible.
Plasma Separation and RBC Lysis : The blood sample was centrifuged at 100 g for 10 minutes, separating the plasma from blood cells. The plasma layer was carefully removed and discarded. The remaining blood cells were mixed with eBioscience™ 1X RBC Lysis Buffer (Invitrogen, Middlesex County, Massachusetts, United States) to achieve a total volume of 10 ml. The mixture was centrifuged at 1500 g for 10 minutes to pellet the WBCs. Despite the RBC Lysis step provided in the FavorPrep™ kit, residual red blood cells were observed. Therefore, an additional lysis step was performed using the same buffer to enhance the purity of the WBC preparation.

Genomic DNA Extraction : The purified WBC pellet obtained from the above steps was used for gDNA isolation. The FavorPrep™ Blood / Cultured Cell Genomic DNA Extraction Mini Kit was employed, following the manufacturer's instructions. This kit ensured efficient and reliable extraction of high-quality gDNA, suitable for various genetic analyses.

2.4 Isolation of Human Peripheral Blood Mononuclear Cells (PBMC)

Detailed steps Peripheral blood mononuclear cells (PBMCs) were isolated from patient blood samples using the Ficoll density gradient centrifugation technique. A preliminary study was conducted to optimize the process prior to the main experiment. The following steps outline the

procedure

Blood Collection : A 6 ml sample of whole blood was collected from the patient into an EDTA tube designed for anticoagulation.

PBMC Isolation : Reagents were prepared with Lymphoprep™ (STEMCELL Technologies, Vancouver, Canada), a density gradient medium optimized for PBMC isolation. The blood sample was combined with the prepared reagents and processed using SepMate™ tubes (STEMCELL Technologies, Vancouver, Canada), which streamline the Ficoll density gradient centrifugation process (Figure 2). The mixture, containing plasma and PBMCs, was centrifuged at 1500 g for 10 minutes to separate the mononuclear cells. After centrifugation, PBMCs were counted using a hemocytometer. A total of $5x10^6$ cells were counted and prepared for storage. For long-term preservation, the PBMCs were resuspended in CryoStor® CS10 (STEMCELL Technologies, Vancouver, Canada), a cryoprotectant medium, and stored under appropriate conditions.

PBMC Preparation for Reprogramming : PBMCs were immediately transferred to a Petri dish containing StemSpan™ SFEM II, a serum-free medium specifically formulated for hematopoietic cell culture and expansion (STEMCELL Technologies, Vancouver, Canada). The medium was supplemented with StemSpan™ Erythroid Expansion Supplement (100X) (STEMCELL Technologies, Vancouver, Canada) to support optimal cell proliferation. Care was taken to ensure that the cells floated atop the medium rather than adhering to the surface, which is critical for maintaining the cells in an optimal state for reprogramming.

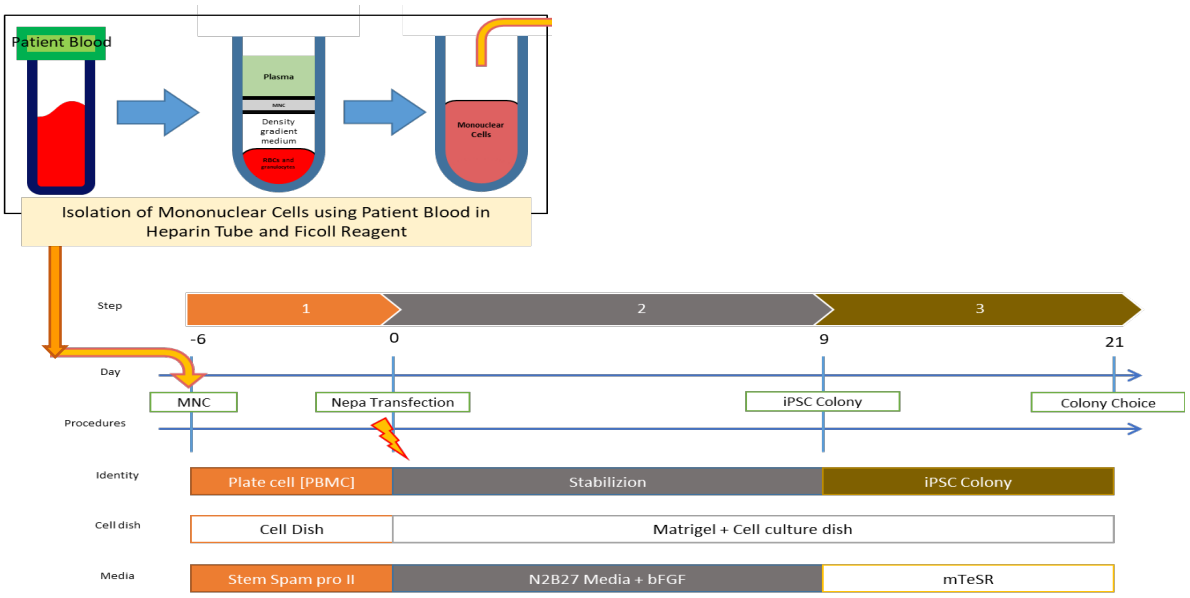

Figure 2. The timeline for generating induced pluripotent stem cells (iPSCs) from mononuclear cells begins with the isolation of mononuclear cells using the Ficoll density gradient method. These cells are then cultured in appropriate conditions for six days to prepare them for reprogramming. Following this, episomal reprogramming factors are introduced via electroporation, after which the cells are transferred to Matrigel-coated plates in a specialized medium to support pluripotency. Over the next 15 days, colonies resembling iPSCs are observed, manually selected, and expanded for further characterization.

2.5 Human Peripheral Blood Mononuclear Cell (PBMC) Culture - Optimization of PBMC culture conditions using defined media and supplements to maintain cell viability and promote expansion.

If PBMC isolation was performed and the cells were frozen, add Dulbecco's Phosphate Buffered Saline (DPBS) at a ratio of 1:9, mix well, and centrifuge at 1600 rpm for 3 minutes to separate them. The subsequent steps are the same as those described below. If proceeding directly

after isolation, add 2 ml of StemSpan™ SFEM II to 2 ul of StemSpan™ Erythroid Expansion Supplement (100X) and culture $5x10^6$ PBMCs for 6 days. The culture medium is a combination of StemSpan™ SFEM II and StemSpan™ Erythroid Expansion Supplement (100X), and the medium should be changed every 2 days for a total of 6 days. (Figure 2)

2.6 iPSCs Reprogramming - Reprogramming Peripheral Blood Mononuclear Cells into iPSCs using episomal vectors or viral methods, including details of the efficiency and safety measures.

Reprogramming Overview : Reprogramming was conducted using the Epi5™ Episomal iPSC Reprogramming Kit (Invitrogen, Middlesex County, Massachusetts, United States), which utilizes episomal vectors encoding specific reprogramming factors to generate integration-free iPSCs. This approach ensures safety and efficiency in reprogramming.

Monocyte Culture Preparation : Monocytes derived from *SCN8A* patients were cultured for 6 days in a medium composed of StemSpan™ SFEM II and StemSpan™ Erythroid Expansion Supplement (100X) (STEMCELL Technologies, Vancouver, Canada). This step was critical for preparing the cells for successful reprogramming.

Cell Resuspension : Following the incubation period, the monocytes were collected and resuspended in 100 µl of Opti-MEM™ I Reduced Serum Medium (Invitrogen, Middlesex County, Massachusetts, United States). This medium was chosen for its ability to enhance transfection efficiency during electroporation.

Introduction of Reprogramming Vectors : To initiate reprogramming, the following vectors were added to the cell suspension in equal volumes (1 µl each): Epi5™ Reprogramming Vectors, Epi5™ p53 & EBNA Vectors. These vectors encode essential reprogramming factors and facilitate episomal reprogramming of the monocytes into iPSCs.

Electroporation : Electroporation was performed using the NEPA21 Super

Electroporator (NEPA GENE, Shiba, Japan). Parameters for the electroporation process were adjusted according to the manufacturer's Epi5™ Kit guidelines, ensuring high cell viability and transfection efficiency. The detailed experimental setup and findings are documented in Table 2. Among these parameters, the porting pulse was configured with a voltage of 150 V, a duration of 5 ms, an interval of 50 ms, sequence number 2, and a duty cycle of 10% with positive polarity. For the transfer pulse, the voltage was set to 20 V, the duration to 50 ms, the interval to 50 ms, sequence number 5, and a duty cycle of 40% with alternating positive and negative polarity. Electroporation was subsequently conducted under these conditions. The measurements revealed that the resistance value exceeded 0.5 kΩ, the porting pulse reached values above 3 A and 5 J, and the transfer pulse surpassed 0.5 A and 1 J.

To prepare the culture environment, Corning® Matrigel® Basement Membrane Matrix, LDEV-free (Corning, Corning, New York, United States), was mixed with Dulbecco's Modified Eagle Medium F12 (DMEM F12) (Invitrogen, Middlesex County, The Commonwealth of Massachusetts, United States) at a 1:90 ratio. This mixture was used to pre-coat the cell culture dish one day prior to use. The culture medium consisted of Neurobasal™ Medium (Invitrogen, Middlesex County, The Commonwealth of Massachusetts, United States), N-2 Supplement (100X) (Invitrogen, Middlesex County, The Commonwealth of Massachusetts, United States), and B-27™ Supplement (50X) (Invitrogen, Middlesex County, The Commonwealth of Massachusetts, United States), all of which are serum-free. To mitigate potential cell damage caused by electroporation, Y-27632 dihydrochloride (MedCamExpress, Monmouth Junction, New Jersey, United States) was added at a concentration of 10 nM.

After preparation, the electroporated PBMCs were added to the pre-coated dish and incubated for a period of 6 to 15 days. The previously prepared culture medium was supplemented with Basic Fibroblast Growth Factor (Merck, Darmstadt, Germany) to achieve a final

concentration of 100 ng/mL. During the incubation period, between days 6 and 15, colonies resembling human embryonic stem cells (hESCs) were visually examined. These colonies were manually harvested using precise mechanical techniques and subsequently cultured for further characterization, as shown in Figure 2.

Table 2. NEPA21 composition table

	Set Parameters Porting Pulse					
	V	Length (ms)	Interval (ms)	No.	Drate (%)	Polarity
Control (with cells and DNA but no electroporation)						
1	100	5	50	2	10	+
2	125	2.5	50	2	10	+
3	125	5	50	2	10	+
4	125	7.5	50	2	10	+
5	150	2.5	50	2	10	+
6	150	5	50	2	10	+
7	150	7.5	50	2	10	+
8	175	5	50	2	10	+
9	200	5	50	2	10	+
10	225	2.5	50	2	10	+
11	275	1	50	2	10	+
	Set Parameters Trans Pulse					
	V	Length (ms)	Interval (ms)	No.	Drate (%)	Polarity
1	20	50	50	5	4	+/-
2	20	50	50	5	4	+/-
3	20	50	50	5	4	+/-
4	20	50	50	5	4	+/-
5	20	50	50	5	4	+/-
6	20	50	50	5	4	+/-
7	20	50	50	5	4	+/-
8	20	50	50	5	4	+/-
9	20	50	50	5	4	+/-
10	20	50	50	5	4	+/-
11	20	50	50	5	4	+/-

2.7 iPSCs Culture - Maintenance of iPSCs in feeder-free conditions with appropriate media and routine monitoring for pluripotency markers.

Human wild-type *SCN8A* iPSCs derived from episomal vectors were maintained in mTeSR™1 (STEMCELL Technologies, Vancouver, Canada). Under feeder-free conditions, as described previously, iPSCs were cultured in Matrigel-coated dishes using mTeSR™1 medium instead of the traditional hESC medium.

In these cell culture conditions, iPSCs were seeded at an initial density of $1x10^5$ cells per 35π Matrigel-coated dish. The culture medium was replaced daily. For thawing frozen cells or performing subcultures, CEPT Cocktail was used to minimize cellular damage. The cocktail included Chroman 1 (MedCamExpress, Monmouth Junction, New Jersey, United States), Emricasan (MedCamExpress, Monmouth Junction, New Jersey, United States), Polyamine Supplement (1000×) (Sigma-Aldrich, St. Louis, Missouri, United States), and Trans-ISRIB (MedCamExpress, Monmouth Junction, New Jersey, United States) to enhance the viability and proliferation of self-renewing pluripotent stem cells and their differentiated progeny in stem cell research applications.

The maximum duration for cell growth was limited to 5 days, and subcultures were performed when cell confluence exceeded 80% of the dish area. The freezing medium used during subculturing consisted of mTeSR1 (40%), KnockOut™ Serum Replacement (KOSR) (50%) (Invitrogen, Middlesex County, The Commonwealth of Massachusetts, United States), and Dimethyl Sulfoxide (DMSO) (10%) (Sigma-Aldrich, St. Louis, Missouri, United States).

For subculturing, cells were detached using ReLeSR™ (STEMCELL Technologies, Vancouver, Canada), following the manufacturer's instructions. Cells were transferred to a new 35π dish at a ratio of 1:10. To stabilize the culture, at least five passages were performed. Additional 2-3 passages were conducted if the cells displayed suboptimal growth or poor

condition.

The remaining cells were stored initially at -20℃ for one day in the prepared freezing medium, then transferred to a deep freezer set at -70℃ to -80℃ for one or more days for long-term storage. Subsequently, the cells were transferred to a liquid nitrogen storage facility for extended preservation.

2.8 Differentiation into Three Germ Layers - Protocols for *in vitro* differentiation of iPSCs into endoderm, mesoderm, and ectoderm, including verification through immunostaining.

To evaluate the capacity of iPSCs for *in vitro* differentiation into the three germ layers, embryoid bodies (EBs) were generated by partial dissociation of iPSCs. For this process, AggreWell™800 (STEMCELL Technologies, Vancouver, Canada) was employed [Sa et al, 2012].

Initially, 500 µl of Anti-Adherence Rinsing Solution (STEMCELL Technologies, Vancouver, Canada) was added to the wells and allowed to sit at room temperature for 5 minutes before centrifugation at 100 g for 3 minutes. After aspirating the rinsing solution, 500 µl of mTeSR™1 medium combined with 0.5 µl of CEPT Cocktail was introduced. iPSCs were seeded at a density of $1x10^6$ cells per well, and after 24 hours of incubation, EBs were visibly formed.

To support further differentiation, a mixture containing 20% KnockOut™ Serum Replacement (KOSR) (Invitrogen, Middlesex County, The Commonwealth of Massachusetts, United States), 1% Penicillin-Streptomycin (10,000 U/mL) (Invitrogen, Middlesex County, The Commonwealth of Massachusetts, United States), 1% MEM Non-Essential Amino Acids Solution (100X) (Invitrogen, Middlesex County, The Commonwealth of Massachusetts, United States), and 1% 2-Mercaptoethanol (Sigma-Aldrich, St. Louis, Missouri, United States) in DMEM/F12 medium was added. Over the course of 6 days, 0.5 ml of medium was replaced daily with fresh EB medium to maintain a total volume of 1 ml.

After the 6-day differentiation phase, the EBs were transferred to Matrigel®-coated dishes for extended culture spanning 14-21 days. Immunostaining with specific antibodies confirmed the spontaneous differentiation of EBs into derivatives of the three germ layers, validating their tri-lineage differentiation potential (Table 3).

Table 3. Antibodies available for the three germ layers.

Antibody	Dilution	Company, Location, CAT No.
Recombinant Anti-PAX6 antibody	1:350	ABCAM, Cambridge, United Kingdom, #EPR15858
Anti-Tubulin Antibody, beta III isoform, CT, clone TU-20 (Similar to TUJ1)	1:500	Merck Millipore, Burlington, Massachusetts, United States MAB1637
Recombinant Anti-Brachyury / Bry antibody	1:1000	ABCAM, Cambridge, United Kingdom, #EPR18113
Alpha-Smooth Muscle Actin Monoclonal Antibody (1A4)	1:1000	Invitrogen, Middlesex County, Massachusetts, United States #14-9760-80
AFP Monoclonal Antibody (F1-6P2A8-P2B9A9)	1:200	Invitrogen, Middlesex County, Massachusetts, United States #MA5-14665
FOXA2 Recombinant Rabbit Monoclonal Antibody (9H5L7)	1:100	Invitrogen, Middlesex County, Massachusetts, United States #701698
Goat anti-Mouse IgG (H+L) Cross-Adsorbed Secondary Antibody, Alexa Fluor™ 568	1:500	Invitrogen, Middlesex County, Massachusetts, United States #A-11004
Goat anti-Rabbit IgG (H+L) Cross-Adsorbed Secondary Antibody, Alexa Fluor™ 488	1:500	Invitrogen, Middlesex County, Massachusetts, United States #A-11008

2.9 Genome DNA Extraction in iPSCs and Identification of Variants - Procedures for extracting gDNA from iPSCs and identifying genetic variants using PCR and sequencing.

DNA Extraction : gDNA was extracted from intracellular nuclei using the Blood & Cell

Culture DNA Midi Kit (QIAGEN, Hilden, Germany) following the protocol provided by the manufacturer. This process ensures high-quality DNA suitable for downstream applications.

iPSC Passaging and Expansion : Patient-specific iPSCs underwent at least five passages to stabilize their growth and characteristics. Once the cell population reached sufficient density, subculturing was performed. Specifically, iPSCs were expanded when their number exceeded $1x10^6$ cells, while monocytes were cultured until $1x10^7$ cells were collected. Before subculturing, cells were treated with Accutase® solution (Sigma-Aldrich, St. Louis, Missouri, United States) for approximately 10 minutes to dissociate them into single cells. The dissociated cells were then counted using a hemocytometer to ensure accurate cell density for subsequent applications.

PCR for Mutation Identification : The extracted gDNA was subjected to polymerase chain reaction (PCR) to determine the precise location of genetic mutations using primers listed in Table 4. PCR was conducted with AccuPower® Taq PCR PreMix (Bioneer, Daejeon, Republic of Korea). Each reaction contained 10 pmol of the predefined primers and 500 ng/μl of gDNA. The thermal cycling conditions included: Pre-denaturation: 95℃ for 5 minutes (1 cycle), Denaturation: 95℃ for 30 seconds, Annealing: 53℃ for 30 seconds, Extension: 72℃ for 1 minute, Final extension: 72℃ for 5 minutes (1 cycle)

The PCR process was repeated for a total of 35 cycles, ensuring amplification of the target DNA regions for mutation analysis. The results were subsequently analyzed to confirm the location and nature of the mutations.

Table 4. PCR primer sequencing of mutation locations of 8AKSW

Name	Primer sequence (5` → 3`)	Tm(℃)	Base pair (bp)
8AKSW F	5′-CCTCCCAAAGTCCTGGGATTACA-3′	65.5	327 bp
8AKSW R	5′-AGCAGGGTACGAATCCCTTT-3′	60.0	

2.10 Identify Sequencing Locations after Gel Extraction Steps for gel electrophoresis-based extraction of PCR products and sequencing to confirm mutation locations.

Agarose Gel Electrophoresis and DNA Extraction : An agarose gel was prepared using 0.5x Tris-acetate-EDTA (TAE) buffer (Sigma-Aldrich, St. Louis, Missouri, United States) and agarose powder (Sigma-Aldrich, St. Louis, Missouri, United States) at a 2% concentration. The gel was cast and allowed to solidify before loading DNA samples. Electrophoresis was conducted at a constant voltage of 135 V for 35 minutes to separate DNA fragments based on size.

Upon visualizing the gel under UV illumination, a DNA band corresponding to 738 bp was identified. This band was carefully excised from the gel using a sterile scalpel. The excised gel fragment containing the DNA of interest was processed for purification using the DNA Fragment Purification Kits - Gel/PCR Purification & Clean-up (Favorgen, Ping Tung, Taiwan), following the manufacturer's protocol.

Sanger Sequencing : The purified DNA was sent to BIONICS (Seoul, Republic of Korea) for Sanger sequencing. This sequencing analysis confirmed the location and specific mutation pattern present in the patient's DNA, providing precise insights into the genetic variation.

2.11 Karyotyping - Analysis of chromosomal integrity in iPSCs to ensure stability and detect potential abnormalities.

G-banding karyotyping was conducted at passage 20 to assess chromosomal integrity and stability. The analysis was performed by DX&VX (Seoul, Republic of Korea) following a standard protocol for GTG (Giemsa-Trypsin-Giemsa) banding. A total of 20 passages were evaluated at a resolution of 550 bands per haploid set, ensuring detailed chromosomal examination and the detection of potential structural abnormalities or numerical changes.

2.12 Immunocytochemistry - Immunostaining techniques for detecting specific markers in differentiated cells and iPSCs.

Immunocytochemistry Protocol for iPSCs : iPSCs were fixed using 4% paraformaldehyde in phosphate-buffered saline (PBS) for 15 minutes at room temperature to preserve cellular structures. Following fixation, the cells were washed thoroughly with PBS to remove residual fixative. Permeabilization was achieved by treating the cells with PBS containing 0.1% Triton X-100 for 15 minutes at room temperature to allow antibody access to intracellular targets.

The samples were then incubated in a blocking buffer composed of PBS supplemented with 2% bovine serum albumin (BSA) (Sigma-Aldrich, St. Louis, Missouri, United States) for 1 hour to minimize nonspecific antibody binding. Subsequently, the cells were incubated overnight at 4°C with primary antibodies diluted in the blocking buffer, targeting specific cellular markers of interest. The next day, the cells were washed three times with PBS to remove unbound primary antibodies and then incubated with fluorescently conjugated secondary antibodies in blocking buffer for 2 hours at room temperature. After incubation, the samples were washed three times with PBS to eliminate excess secondary antibodies. Cover slips were then mounted onto

microscope slides using VECTASHIELD® Antifade Mounting Medium (VectorBuilder, Chicago, Illinois, United States) containing DAPI for nuclear staining. For applications requiring mounting without DAPI, VECTASHIELD® Mounting Medium (VectorBuilder, Chicago, Illinois, United States) was used.

Fluorescence Imaging : Fluorescence imaging was performed using a pE-300lite LED fluorometer (Olympus, Tokyo, Japan) and a fluorometer equipped with TH4-200 illumination (Olympus, Tokyo, Japan). All fluorescence images were captured with an IX74 microscope (Olympus, Tokyo, Japan) equipped with a DP74 digital camera (Olympus, Tokyo, Japan) for high-resolution imaging. (Table 3)

2.13 STR Analysis Short Tandem Repeat (STR) profiling to authenticate cell lines and verify their identity.

STR analysis was employed to compare allelic repeats at specific loci in DNA across two or more samples, ensuring the genetic identity and stability of the samples. The analysis was conducted by Cosmogentech Inc. (Seoul, Republic of Korea) and repeated twice for confirmation. First Comparison: The gDNA extracted from the patient's mononuclear cells was compared to the gDNA extracted from the patient's iPSCs. This step validated that the iPSCs retained the genetic identity of the donor cells.

Second Comparison: The gDNA extracted from the calibrated iPSCs was compared to the gDNA from the same iPSCs at passage 10. This comparison ensured the genetic consistency and stability of the iPSCs during culture and expansion.

For all analyses, iPSCs were harvested at passage 10 to provide sufficient material for the study. STR profiles were generated and analyzed to confirm the match and rule out contamination or unintended genetic changes during reprogramming and culture.

2.14 Prime Editing Strategy for gene editing

To introduce the c.4871T>G mutation into mutant patient-derived iPSCs, prime editing (PE) was performed using the PE2 system. The pegRNA and PE3b sgRNA were cloned into the prime editing plasmids following a two-step cloning procedure.

pegRNA and PE3b sgRNA Design:

The pegRNA was designed to contain a primer binding site (PBS), reverse transcriptase (RT) template, and spacer sequence targeting the mutation site. The sequences used were:

- sgRNA: GACGCAAGATGCGCCCACTA--CGG
- RT template (12 nt): ATTGGCCCGTAT
- PBS (12 nt): TGGGCGCATCTT
- Sense 3' extension forward: ATTGGCCCGTATTGGGCGCATCTT
- Sense 3' extension reverse: AAAAAAGATGCGCCCAATCCTGGCCAAT

The full-length pegRNA sequence was as follows:

GACGCAAGATGCGCCCACTAGTTTTAGAGCTAGAAATAGCAAGTTAAAATAAGGCTAG TCCGTTATCAACTTGAAAAAGTGGCACCGAGTCGGTGCATTGGCCAGGATTGGGCGCA TCTT

The PE3b nicking sgRNA was also designed to facilitate efficient prime editing, with the sequence:

- PE3 sgRNA: CCTCTTCTTAGGAATGTTCC
- PE3b sgRNA: TCATCCGATTGGCCCGTATT

Vector Construction:

The pegRNA and PE3b sgRNA were cloned into the pU6-pegRNA-GG-acceptor (Add gene #132777) plasmid using Golden Gate Assembly, while the PE2 enzyme was delivered using the pCMV-PE2-P2A-GFP (Add gene #132776) plasmid.

Transfection and Prime Editing:

Mutant patient-derived iPSCs were transfected using Lipofectamine Stem Transfection Reagent (or electroporation, if used) following the manufacturer's protocol. Briefly, 10^5 cells were plated in mTeSR1 and transfected with pCMV-PE2-P2A-GFP, pegRNA plasmid, and PE3b sgRNA plasmid. After [insert time] hours, GFP-positive cells were enriched using fluorescence-activated cell sorting (FACS) or antibiotic selection (if applicable).

Genomic DNA Extraction and PCR Amplification:

Genomic DNA was extracted 72 hours post-transfection using the DNeasy Blood & Tissue Kit (QIAGEN). PCR amplification of the target SCN8A locus was performed using the following primers:

- Forward Primer: [5'-CCTCCCAAAGTCCTGGGATTACA-3']
- Reverse Primer: [5’- AGCAGGGTACGAATCCCTTT -3’]

The PCR amplicons were purified using the QIAquick PCR Purification Kit (QIAGEN) and subjected to Sanger sequencing to confirm genome editing.

Sequence Analysis and Alignment:

Edited sequences were aligned to the SCN8A reference sequence (Accession: NM_014191.3) using SnapGene software. Wild-type and edited sequences were compared to evaluate precise base editing.

Wild-type Sequence:

AACTTCTTCTATTCCTCTTCTTAGGAATGTTCCTGGCAGATATAATTGAGAAATACTTTGT TTCCCCAACCCTATTCCGAGTCATCCGATTGGCCCGTAG(mc.4871T>G)TGGGCGCATCT TGCGTCTGATCAAAGGCGCCAAAGGGATTCGTACCCTGCTCTTTGCCTTAATGATGTCC TTGCCTGCCCTGTTCAACATCGGCCTTCTG

Edited Sequence:

AACTTCTTCTATTCCTCTTCTTAGGAATGTTCCTGGCAGATATAATTGAGAAATACTTTGT TTCCCCAACCCTATTCCGAGTCATCCGATTGGCCC(a-silent mutation)GT(g-silent mutation)A T(corrected)TGGGCGCATCTTGCGTCTGATCAAAGGCGCCAAAGG GATTCGTACCCTGCTCTTTGCCTTAATGATGTCCTTGCCTGCCCTGTTCAACATCGGCCT TCTG

The alignment confirmed successful incorporation of the intended c.4871T>G edit.

The prime editing system comprised two plasmids (Figure 3):

1) pU6-pegRNA-GG-acceptor (Addgene #132777) was modified to express the prime editing guide RNA (pegRNA), which included:

- A spacer sequence (5′-GACGCAAGATGCGCCCACTA-3′) targeting the *SCN8A* locus.
- A reverse transcriptase (RT) template (5′-ATTGGCCCGTAT-3′) encoding the c.4871T>G mutation.

- A primer binding site (PBS) (5′-TGGGCGCATCTT-3′) for reverse transcription.
- A PE3b sgRNA (5′-TCATCCGATTGGCCCGTATT-3′) to enable strand-specific nicking.

2) pCMV-PE2-P2A-GFP (Addgene #132776) expressed the PE2 enzyme (a Cas9 nickase fused with engineered reverse transcriptase) and a GFP reporter for transfection efficiency tracking.

The pegRNA and PE3b sgRNA were cloned into the pU6-pegRNA-GG-acceptor plasmid via Golden Gate Assembly. The PE2 plasmid (10,603 bp total length) provided all components necessary for precise editing, including the PE2 enzyme and GFP for fluorescence-activated cell sorting (FACS) enrichment of transfected cells.

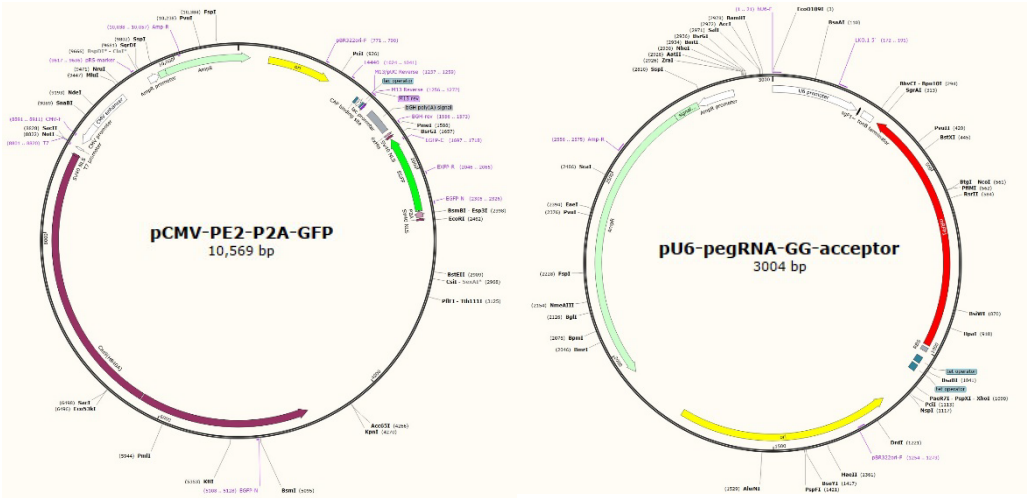

Figure 3. Prime Editing Vector Design. The prime editing system comprised two plasmids.

2.15 Prime Editing-Mediated Heterozygous Indel Mutation in SCN8A

To introduce a heterozygous indel mutation in the *SCN8A* gene at c.4871T>G in an iPSC line derived from an *SCN8A* mutant patient, prime editing (PE) technology was employed. A prime editing guide RNA (pegRNA) was designed to target *SCN8A* specifically, incorporating the desired T>G substitution and a reverse transcriptase template. The pegRNA and a nick sgRNA (ngRNA) were cloned into a prime editing vector (pPE3-Puro-EGFP, VectorBuilder, Chicago, Illinois, United States), encoding a Cas9 nickase-reverse transcriptase fusion protein.

Cell Preparation and Electroporation:

iPSCs were expanded through approximately 10 passages to generate a homogeneous single-cell population using Accutase. Cells were adjusted to a concentration of 1×1061×106 cells in 50 µL Opti-MEM and mixed with 5 µL of the prime editing plasmid. Electroporation was performed using the NEPA21 Electroporator under optimized conditions (Table 2):

- Porating pulse: 125 V, 5 ms pulse length, 5 ms interval, 2 pulses, 10% duty rate, positive polarity
- Transfer pulse: 20 V, 50 ms pulse length, 50 ms interval, 5 pulses, 4% duty rate, alternating polarity

Post-Electroporation Treatment:

To enhance cell survival and editing efficiency, cells were treated with 1 µM Pifithrin-alpha (Sigma-Aldrich) for 24 hours post-electroporation to transiently inhibit p53-mediated apoptosis.

Cell Recovery and Selection:

After nucleofection, cells were resuspended in mTeSR supplemented with CEPT (1/1000 dilution), doxycycline(2μg/ml) and seeded onto Matrigel pre-coated plates. At 48 hours post-electroporation, eGFP-positive cells were sorted via FACS. Puromycin selection (1 μg/mL for 3 days) was applied to enrich for cells successfully transfected with the prime editing construct. Puromycin-resistant colonies were manually picked and expanded for downstream screening.

Mutation Confirmation and Clone Selection:

Sanger sequencing confirmed precise heterozygous editing of c.4871T>G, with three independent clones selected for further characterization. All clones tested negative for mycoplasma contamination.

Pluripotency and Karyotype Assessment:

Immunocytochemistry validated sustained expression of pluripotency markers (OCT4, NANOG, SSEA4, TRA1-81) in the edited iPSCs. Chromosomal stability was confirmed by karyotyping (Dx&Vx Inc.).

Off-Target Analysis:

Potential off-target sites were predicted using pegRNA-specific algorithms (PE-Analyzer and Benchling) with a mismatch tolerance of ≤3 across the pegRNA spacer and template regions. No off-target edits were detected via Sanger sequencing at the top 5 predicted loci.

2.16 Isogenic Cell Culture - Culturing edited and unedited iPSCs to generate isogenic cell lines for comparative studies.

After Prime editing and puromycin selection, the condition of the cells may deteriorate

due to the stress caused by the selection process. To ensure the recovery and purification of edited cells, immediate steps are required.

Cell Transfer and Initial Recovery: After completing puromycin selection, transfer the entire population of cells into 96-well plates. Incubate the cells under appropriate conditions for approximately 5 days to promote recovery and initial growth.

gDNA Extraction and Verification: Once the cells have recovered, divide the population into two halves. One half is used for gDNA extraction, without prior cell counting, to expedite the process. Sanger sequencing is performed on the extracted gDNA to identify successfully edited cells and confirm the presence of the intended mutation.

Expansion of Edited Cells: Successfully edited cells are then transferred to 6-well plates pre-coated with Matrigel for further expansion. The culture medium, mTeSR1 supplemented with CEPT, is added to support cell growth and health.

Culturing and Final Recovery: The cells are cultured in the 6-well plates for an additional 6 days to obtain a healthy and robust cell population suitable for subsequent experiments or analyses.

2.17 Confirmation of Off-Target Effects in Prime Editing - Analysis of potential off-target effects using bioinformatics tools and sequencing

1) Identification of Candidate Off-Target Sites

To evaluate potential off-target effects of the prime editing system, candidate off-target loci were identified using CAS-Offinder (http://www.rgenome.net/cas-offinder/) and Benchling (https://www.benchling.com/).

- Prime Editor-Specific Parameters:

- The pegRNA sequence (including the primer binding site [PBS] and reverse transcription template [RTT]) and the Cas9 nickase (H840A) scaffold were analyzed for potential off-target binding.
- Mismatch tolerance was set to ≤3 nucleotides in the PBS and RTT regions, with bulges allowed (up to 1 bp) to account for pegRNA flexibility.
- Sites with a predicted off-target score ≥1 (based on sequence homology and predicted binding energy) were prioritized.

- RNA Off-Targets: Potential interactions between the pegRNA and non-target genomic regions were assessed using RNA:DNA hybridization prediction tools (e.g., PINESA).

2) Primer Design for Off-Target Amplification

For each prioritized off-target locus:

- Primers were designed using Primer 3 or Benchling's Primer Design Tool to amplify genomic regions spanning the predicted off-target site.
- Specificity: Primer pairs were optimized to avoid secondary structures and cross-hybridization, ensuring amplification of only the intended locus.
- Amplicon Size: Fragments of 300–500 bp were targeted to facilitate Sanger sequencing resolution.

3) Validation via Sanger Sequencing

- PCR Amplification: Genomic DNA from edited and unedited (control) cells was amplified using the designed primers.
- Sequencing: Purified PCR products were subjected to Sanger sequencing.

- Analysis:
    - Sequencing traces were aligned to reference sequences using SnapGene or Benchling to identify insertions, deletions, or mismatches.
    - PE-specific artifacts: Special attention was paid to low-frequency edits (<5% frequency) and unintended nicking events, which are less common in prime editing compared to Cas9 nuclease-based systems.

4) Computational Confirmation of Editing Precision

- Prime Editing Efficiency: On-target editing efficiency and purity were quantified using ICE Analysis (Synthego) or TIDE to ensure high-fidelity edits.
- Off-Target Likelihood: Sites with no detectable edits via sequencing were further analyzed using in silico tools (e.g., DeepPrime or PE-Analyzer) to predict PE activity at mismatched loci.

2.18 Lenti-Virus Design - Development of lentiviral vectors for gene delivery in various experimental applications.

To guide the differentiation of iPSCs into specific neuronal subtypes, transcription factors were expressed to direct differentiation toward either inhibitory GABAergic neurons or excitatory glutamatergic neurons, mimicking the forebrain cortical environment.

Lenti Virus Design for GABAergic Neurons: The Tet-On system was utilized to achieve inducible expression of the transcription factors ASCL1 and DLX2, which promote the differentiation of GABAergic neurons. RFP (Red Fluorescent Protein) was incorporated into the lentiviral vector to verify successful viral transduction through fluorescence microscopy. An Anti-

Puromycin (Anti-Puro) selection marker was included to eliminate non-infected cells, ensuring a pure population of transduced cells.

Lenti Virus Design for Glutamatergic Neurons: The transcription factor Neurog2 (NGN2), essential for excitatory glutamatergic neuron differentiation, was added to the lentiviral vector. eGFP (Enhanced Green Fluorescent Protein) was used as a marker to confirm viral transduction through fluorescence imaging. Similar to the GABAergic neuron protocol, Anti-Puro was used for selection.

rtTA Vector Design: A separate lentiviral vector was designed for the reverse tetracycline transactivator (rtTA) system, enabling inducible control of the Tet-On system. This vector was created without selection markers to allow flexibility in co-expression studies.

Lenti Virus Construction: All lentiviral constructs were designed using VectorBuilder. The design details, including sequences, cloning strategies, and vector maps, are documented in Tables 5–10. This method ensures precise and efficient differentiation into GABAergic and glutamatergic neurons, facilitating downstream studies in a forebrain cortex-like environment.

Table 5. Information about Lenti-virus (ASCL1+DLX2)

Name	Position	Size (bp)	Type	Description	Application notes
RSV promoter	1–229	229	Promoter	Rous sarcoma virus enhancer/promoter	Strong promoter; drives transcription of viral RNA in packaging cells.
Δ5' LTR	230–410	181	LTR	Truncated HIV-1 5' long terminal repeat	Allows transcription of viral RNA and its packaging into virus.
Ψ	521–565	45	Miscellaneous	HIV-1 packaging signal	Allows packaging of viral RNA into virus.
RRE	1075–1308	234	Miscellaneous	HIV-1 Rev response element	Rev protein binding site that allows Rev-dependent nuclear export of viral RNA during viral packaging.

cPPT	1803–1920	118	Miscellaneous	Central polypurine tract	Facilitates the nuclear import of HIV-1 cDNA through a central DNA flap.
EF1A	1959–3137	1179	Promoter	Human eukaryotic translation elongation factor 1 α1 promoter	Strong promoter.
Kozak	3162–3167	6	Miscellaneous	Kozak	Facilitates translation initiation.
mCherry	3168–3878	711	CDS	Variant of mRFP1 generated by mutagenesis	Commonly used red fluorescent protein; fast maturation compared to its predecessor, mRFP1.
WPRE	3917–4514	598	Miscellaneous	Woodchuck hepatitis virus posttranscriptional regulatory element	Enhances viral RNA stability in packaging cells, leading to higher titer of packaged virus.
CMV promoter	4536–5123	588	Promoter	Human cytomegalovirus immediate early enhancer/promoter	Strong promoter; may have variable strength in some cell types.
EGFP:T2A:Puro	5155–6534	1380	CDS	EGFP and Puro linked by T2A	Allows cells to be visualized by green fluorescence and resistant to puromycin.
ΔU3/3' LTR	6605–6839	235	LTR	Truncated HIV-1 3' long terminal repeat	Allows packaging of viral RNA into virus; self-inactivates the 5' LTR by a copying mechanism during viral genome integration; contains polyadenylation signal for transcription termination.
SV40 early pA	6912–7046	135	PolyA_signal	Simian virus 40 early polyadenylation signal	Allows transcription termination and polyadenylation of mRNA transcribed by Pol II RNA polymerase.
Ampicillin	8000–8860	861	CDS	Ampicillin resistance gene	Allows E. coli to be resistant to ampicillin.
pUC ori	9031–9619	589	Replication_origin	pUC origin of replication	Facilitates plasmid replication in E. coli; regulates high-copy plasmid number (500-700).

Table 6. Lenti-virus (ASCL1+DLX2) summary

Title	Information
Vector ID:	VB220823-1096trw
Vector Name:	pLV[Exp]-mCherry:T2A:Puro-TRE>hASCL1[NM_004316.4](ns):T2A:hDLX2[NM_004405.4]
Vector Type:	Mammalian Tet Inducible Gene Expression Lentiviral Vector
Vector Size:	10368 bp
Viral Genome Size:	6893 bp
Promoter:	TRE
ORF:	hASCL1[NM_004316.4](ns), hDLX2[NM_004405.4]
Linker:	T2A
Marker:	mCherry:T2A:Puro
Plasmid Copy Number:	High
Antibiotic Resistance:	Ampicillin

Table 7. Information about Lenti-virus (NGN2)

Name	Position	Size (bp)	Type	Description	Application notes
RSV promoter	1–229	229	Promoter	Rous sarcoma virus enhancer/promoter	Strong promoter; drives transcription of viral RNA in packaging cells.
5' LTR-ΔU3	230–410	181	LTR	Truncated HIV-1 5' long terminal repeat	Allows transcription of viral RNA and its packaging into virus.
Ψ	521–565	45	Miscellaneous	HIV-1 packaging signal	Allows packaging of viral RNA into virus.
RRE	1075–1308	234	Miscellaneous	HIV-1 Rev response element	Rev protein binding site that allows Rev-dependent nuclear export of viral RNA during viral packaging.
cPPT	1803–1920	118	Miscellaneous	Central polypurine tract	Facilitates the nuclear import of HIV-1 cDNA through a central DNA flap.
TRE	1959–2382	424	Promoter	Tetracycline-responsive element promoter (2nd generation)	Regulated by a class of transcription factors (e.g. tTA, rtTA and tTS) whose activities are dependent on tetracycline or its analogs (e.g. doxycycline).
Kozak	2407–2412	6	Miscellaneous	Kozak translation initiation sequence	Facilitates translation initiation of ATG start codon downstream of the Kozak sequence.
hNEUROG2 [NM_024019.4]	2413–3231	819	CDS	None	None
WPRE	3270–3867	598	Miscellaneous	Woodchuck hepatitis virus posttranscriptional regulatory element	Enhances virus stability in packaging cells, leading to higher titer of packaged virus; enhances higher expression of transgenes.
CMV promoter	3889–4476	588	Promoter	Human cytomegalovirus immediate early enhancer/promoter.	Strong promoter; may have variable strength in some cell types.
EGFP:T2A: Puro	4508–5887	1380	CDS	EGFP and Puro linked by T2A	Allows cells to be visualized by green fluorescence and resistant to puromycin.
3' LTR-ΔU3	5958–6192	235	LTR	Truncated HIV-1 3' long terminal repeat	Allows packaging of viral RNA into virus; self-inactivates the 5' LTR by a copying mechanism during viral genome integration; contains polyadenylation signal for transcription termination.
SV40 early pA	6265–6399	135	PolyA_signal	Simian virus 40 early polyadenylation signal	Allows transcription termination and polyadenylation of mRNA transcribed by Pol II RNA polymerase.

AmpiciIIin	7353–8213	861	CDS	AmpiciIIin resistance gene	Allows E. coli to be resistant to ampiciIIin.
pUC ori	8384–8972	589	Rep_origin	pUC origin of replication	Facilitates plasmid replication in E. coli; regulates high-copy plasmid number (500-700).

Table 8. Lenti-virus (NGN2) summary

Title	Information
Vector ID:	VB220823-1048fty
Vector Name:	pLV[Exp]-EGFP:T2A:Puro-TRE >hNEUROG2[NM_024019.4]
Vector Type:	Mammalian Tet Inducible Gene Expression Lentiviral Vector
Vector Size:	9438 bp
Viral Genome Size:	5963 bp
Promoter:	TRE
ORF:	hNEUROG2[NM_024019.4]
Marker:	EGFP:T2A:Puro
Plasmid Copy Number:	High
Antibiotic Resistance:	Ampicillin

Table 9. Information about Lenti-virus (rtTA)

Name	Position	Size (bp)	Type	Description	Application notes
RSV promoter	1–229	229	Promoter	Rous sarcoma virus enhancer/promoter	Strong promoter; drives transcription of viral RNA in packaging cells.
Δ5' LTR	230–410	181	LTR	Truncated HIV-1 5' long terminal repeat	Allows transcription of viral RNA and its packaging into virus.
Ψ	521–565	45	Miscellaneous	HIV-1 packaging signal	Allows packaging of viral RNA into virus.
RRE	1075–1308	234	Miscellaneous	HIV-1 Rev response element	Rev protein binding site that allows Rev-dependent nuclear export of viral RNA during viral packaging.
cPPT	1803–1920	118	Miscellaneous	Central polypurine tract	Facilitates the nuclear import of HIV-1 cDNA through a central DNA flap.
UBC	1959–3136	1178	Promoter	Human ubiquitin C promoter	Weak promoter.
Kozak	3161–3166	6	Miscellaneous	Kozak translation initiation sequence	Facilitates translation initiation of ATG start codon downstream of the Kozak sequence.
rtTA	3167–3913	747	CDS	Reverse tetracycline responsive transcriptional activator M2 (2nd generation)	It binds to TRE promoter to activate gene transcription only in the presence of tetracycline or its analogs (e.g. doxycycline). It has higher sensitivity to the inducing drug and lower leaky activity in the absence of the drug compared to its predecessor, rtTA.
WPRE	3952–4549	598	Miscellaneous	Woodchuck hepatitis virus posttranscriptional regulatory element	Enhances virus stability in packaging cells, leading to higher titer of packaged virus; enhances higher expression of transgenes.
ΔU3/3' LTR	4631–4865	235	LTR	Truncated HIV-1 3' long terminal repeat	Allows packaging of viral RNA into virus; self-inactivates the 5' LTR by a copying mechanism during viral genome integration; contains polyadenylation signal for transcription termination.
SV40 early pA	4938–5072	135	PolyA_signal	Simian virus 40 early polyadenylation signal	Allows transcription termination and polyadenylation of mRNA transcribed by Pol II RNA polymerase.
Ampicillin	6026–6886	861	CDS	Ampicillin resistance gene	Allows E. coli to be resistant to ampicillin.
pUC ori	7057–7645	589	Rep_origin	pUC origin of replication	Facilitates plasmid replication in E. coli; regulates high-copy plasmid number (500-700).

Table 10. Lenti-virus (rtTA) summary

Title	Information
Vector ID:	VB010000-4667vsp
Vector Name:	pLV[Exp]-UBC>rtTA
Vector Type:	Tet Regulatory Protein Expression Lentiviral Vector
Vector Size:	8111 bp
Viral Genome Size:	4636 bp
Promoter:	UBC
ORF:	rtTA
Plasmid Copy Number:	High
Antibiotic Resistance:	Ampicillin

2.19 Neuron Differentiation - Differentiation of iPSCs into functional neurons using defined protocols and supplements.

iPSC Seeding and Virus Infection : To initiate neuronal differentiation, $1x10^7$ iPSCs were seeded into a 35π Matrigel-coated culture dish. The cells were allowed to grow for at least one day to reach optimal density. Once the cells were ready, 1 titer of Lenti Virus containing the transcription factor of interest and 1 titer of Lenti Virus containing rtTA were added to the culture. Media Replacement : Approximately 16 hours after virus infection, the medium was replaced with Neuronal Growth Medium (NGM Media). This medium was formulated to support neuronal growth and differentiation and included the following components: The neuronal culture medium was prepared using Neurobasal Plus as the base medium, supplemented with several key components to ensure optimal cell viability and functionality. N2 Serum-Free Supplement (1x) and B-27™ Plus Supplement (1x) were added to provide essential nutrients and support cell viability. To protect against oxidative damage, L-Ascorbic Acid was included at a concentration of 100 μM.

To promote neuronal survival and synaptic development, neurotrophic factors BDNF (Brain-Derived Neurotrophic Factor) and GDNF (Glial Cell-Derived Neurotrophic Factor) were

added at a concentration of 10 ng/µl each. Bucladesine Sodium (dbcAMP) was incorporated at 250 µM to enhance neuronal activity and support signaling pathways critical for neuronal function. Additionally, GlutaMAX™ Supplement (1x) was used to stabilize L-glutamine levels, reducing ammonia buildup and ensuring a stable environment for neuronal growth and maintenance. Doxycycline monohydrate was also added at a final concentration of 1 µg/ml, and the cells were incubated for one day.

Fluorescence and Selection : After 24 hours, the cells were examined under a microscope for fluorescence expression to verify virus infection. Once fluorescence was confirmed, puromycin was added at a final concentration of 1 µg/ml for three days to select successfully transduced cells.

Post-Selection Treatments : Following the selection process, the cells were treated with the following: To optimize neuronal differentiation and inhibit the proliferation of non-neuronal cells, specific additives were included in the culture protocol. β-D-Arabinofuranosylcytosine (Ara-C) was applied at a concentration of 1 µg/ml for two days to effectively inhibit cell division, particularly targeting non-neuronal cells. Additionally, Forskolin was added at 20 µM for two days to enhance cyclic AMP (cAMP) activity. This increase in cAMP levels plays a crucial role in promoting neuronal differentiation and supporting the maturation of neuronal cells. These measures were implemented to ensure a more efficient and targeted neuronal culture process.

Pre-Co-Culture Preparation : After completing the treatments, the medium was replaced with fresh NGM Media. The cells were incubated for an additional day to stabilize the neuronal populations, preparing them for co-culture or further experimentation.

Methodology Reference and Customization : This protocol was adapted from methodologies described in Nature and Cell journals. The timeline and procedures were customized in the laboratory to improve reproducibility and efficiency, ensuring optimal outcomes for neuronal

differentiation.

2.20 Neuron Culture - Maintenance and expansion of neurons in culture for downstream analyses.

Day 1 – Doxycycline Addition and Media Changes : The first day of neuronal differentiation is marked by the addition of Doxycycline to induce transcription factor expression. The neurons are cultured for approximately 1 week, with daily replacement of the NGM Media to maintain optimal growth and differentiation conditions.

Preparing Astrocyte-Coated Cover-Slips : One day before the neurons reach 1 week of age, cover-slips are prepared in a 24-well plate by coating them with Matrigel. Following this, $1x10^5$ astrocytes are seeded onto the coated cover-slips. These astrocytes facilitate co-culture with the neurons and support their maturation.

Neurons for Patch-Clamp Analysis : To prepare neurons for patch-clamp electrophysiological measurements : On the astrocyte-coated cover-slips, dissociate neurons into single cells using Accutase. Plate $5x10^4$ neurons onto the prepared astrocyte-coated cover-slips. These neurons will be used to study electrophysiological properties through patch-clamp recordings.

Neurons for ICC and cDNA Synthesis : For immunocytochemistry (ICC) and cDNA synthesis: On a separate cover-slip without astrocytes, dissociate neurons into single cells using Accutase. Plate $5x10^4$ neurons onto the cover-slip using NGM Media mixed with Mouse Astrocyte Conditioned Medium at a 10% composition, derived from C57BL/6 mice (ScienCell Research Laboratories, Carlsbad, CA, USA). These neurons will be analyzed for molecular and protein expression.

Preparing for MicroElectrode Array (MEA) Recording : To set up neurons for MEA recordings : One day before the neurons reach 1 week of age, coat an MEA plate with Matrigel

and seed $5x10^4$ astrocytes onto the plate. Add a total of $1x10^5$ neurons to the MEA plate, with the following composition : $1.5x10^4$ GABAergic neurons, $3.5x10^4$ Glutamatergic neurons

- This configuration allows for robust electrophysiological measurements.

Media Maintenance for MEA and Co-Culture : To ensure the neurons remain healthy and functional during MEA recordings and co-culture: Replace 50% of the media with an equal volume of fresh media every 2 days. This partial media change maintains consistent environmental conditions while reducing stress on the neurons.

2.21 Mouse Astrocyte Primary Culture Isolation and culture of primary astrocytes from mouse brains for co-culture experiments.

The following study was conducted in strict adherence to the guidelines set by the Institutional Animal Care and Use Committee (IACUC), approval number 2018-0187, at the Department of Experimental Animals, Severance Hospital, Yonsei University. The experiments utilized the brains of 1-day-old mouse pups, following the protocol described in the publication DOI: 10.3791/50079. This ensured reproducibility and compliance with established methods for experimental rigor and ethical animal research practices.

2.22 mRNA Extraction and cDNA Synthesis

mRNA Extraction: Primary neurons cultured on coverslips (3–7 weeks, astrocyte-free) were harvested at regular intervals. Total RNA was isolated using TRIzol™ Reagent (Sigma-Aldrich, St. Louis, MO, USA) according to the manufacturer's protocol. Briefly, 1 mL TRIzol™ was added directly to cells, followed by 200 µL chloroform (Sigma-Aldrich). After vigorous vortexing, samples were incubated on ice for 15 min and centrifuged at 12,000 × *g* for 10 min

(4°C) to separate phases. The aqueous RNA-containing layer was transferred to a fresh tube, mixed with 500 µL ice-cold 2-propanol (Sigma-Aldrich), and incubated on ice for 10 min. RNA was pelleted by centrifugation (12,000 × *g*, 10 min, 4°C), washed with 1 mL 70% ethanol, and centrifuged again (7,500 × *g*, 10 min, 4°C). The air-dried RNA pellet was resuspended in 50 µL UltraPure™ DEPC-treated water (Invitrogen, Waltham, MA, USA) and stored at −20°C. All steps were performed on ice or at 4°C to preserve RNA integrity.

cDNA Synthesis: RNA concentration was quantified using a Nanodrop spectrophotometer (Thermo Fisher Scientific, Waltham, MA, USA). For reverse transcription, 500 ng RNA was combined with 2 µL 5X PrimeScript™ RT Master Mix (Takara Bio, Kusatsu, Japan) and adjusted to a final volume of 10 µL with DEPC-treated water. Reactions were incubated at 37°C for 15 min, followed by heat inactivation at 85°C for 5 sec. Synthesized cDNA was stored at −20°C for downstream applications.

Neuronal Characterization by PCR: Target cDNA sequences were amplified using AccuPower® Taq PCR PreMix (Bioneer, Daejeon, Korea) in a 20 µL reaction containing 10 pmol gene-specific primers (Table 4) and 500 ng/µL cDNA. Thermal cycling conditions were as follows: initial denaturation at 95°C for 5 min; 35 cycles of denaturation (95°C, 30 sec), annealing (50°C, 30 sec), and extension (72°C, 1 min); and final extension at 72°C for 5 min. Primer sequences were designed using NCBI Primer-BLAST and validated for specificity prior to use. Amplified products were analyzed by agarose gel electrophoresis or sequenced for validation.

2.23 Neuron Characterization (PCR) - Characterization of neuronal identity and subtype using PCR-based analysis.

PCR amplification was carried out to amplify target cDNA using AccuPower® Taq PCR

PreMix (Bioneer, Daejeon, Republic of Korea). The reaction mixture was prepared with the following components to ensure specificity and efficiency: 10 pmol of primers designed specifically for the target cDNA sequence. 500 ng/μl of cDNA synthesized during earlier steps. The thermal cycler program included the following steps:

Pre-denaturation : The reaction mixture was pre-heated at 95°C for 5 minutes (1 cycle) to denature the double-stranded cDNA into single strands, ensuring the primers could access the template for the subsequent steps.

Thermal Cycling (35 cycles) : Thermal cycling was performed for a total of 35 cycles, each consisting of the following stages:

1. Denaturation: Heat the mixture at 95°C for 30 seconds to separate the double-stranded cDNA into single strands.
2. Annealing: Reduce the temperature to 50°C for 30 seconds to allow the primers to hybridize with their complementary sequences on the cDNA template.
3. Extension: Increase the temperature to 72°C for 1 minute to enable Taq polymerase to synthesize the complementary DNA strand by adding nucleotides to the primers.

Final Extension : A final extension step was performed at 72°C for 5 minutes (1 cycle) to ensure that any incomplete DNA strands were fully extended, resulting in complete amplification of the target sequence. Primers were designed to specifically target complementary regions within the cDNA sequence, and their compatibility and accuracy were confirmed before initiating the PCR process. For detailed information on primer sequences, refer to Table 4.

This protocol reliably amplified the target cDNA, producing high-quality DNA for downstream analyses such as sequencing or expression validation. Should any issues arise, optimization steps such as adjusting the annealing temperature or primer concentrations can be employed to enhance performance.

2.24 Multi Electrode Array (MEA) Recordings and Analysis - Measurement of neuronal activity using MEA and analysis of electrophysiological properties.

All recordings were performed using a 24-well MEA system integrated with the Maestro Edge platform from Axion BioSystems, located in Atlanta, Georgia, USA. Neural networks were cultured in the MEA plates with a composition of $1.5x10^4$ GABAergic neurons, $3.5x10^4$ Glutamatergic neurons, and $5x10^4$ Astrocytes, resulting in a total of $1x10^5$ cells per well. This structured neuronal network model was designed to mimic physiological conditions and ensure functional connectivity.

Spontaneous activity of *SCN8A* iPSC-derived neural networks and calibrated *SCN8A* iPSC-derived neural networks was recorded for 15 minutes in a controlled recording chamber maintained at 37°C with 95% O_2 and 5% CO_2. To ensure baseline stabilization and minimize external disturbances, the cultures were acclimatized in the chamber for 10 minutes before recording. The medium was replaced one day before the experiment to avoid mechanical stress on the day of recording.

Signals were sampled at a frequency of 10 kHz to capture high-resolution electrophysiological data. A high-pass filter (100 Hz cutoff) and low-pass filter (3500 Hz cutoff) were applied to refine the recordings and reduce noise. The spike detection threshold was set at ±4.5 standard deviations, providing robust identification of neuronal firing events.

Data analysis was conducted using AxIS, the software module for the Maestro MEA platform, which facilitated real-time data visualization and intuitive workflows. The Mean Firing Rate (MFR), representing the average spike frequency across all channels, was calculated as a standard measure of network activity. Bursts were identified as sequences of at least five spikes occurring with a minimum rate of 0.4 bursts per second and an inter-burst interval of 100 ms.

Network bursts, indicative of synchronized neuronal activity, were defined as burst events occurring in more than 35% of the channels in a single well.

All definitions and measurement parameters strictly adhered to the user guidelines provided by Axion BioSystems. This protocol enabled a detailed evaluation of the electrophysiological behavior of *SCN8A* iPSC-derived neural networks, providing insights into their functional connectivity and activity patterns. (Table 11)

Table 11. MEA definition

Metric	Definition
Number of Spikes	The total number of spikes in the analysis period.
Mean Firing Rate	The total number of spikes divided by the duration of the analysis, in Hz.
Burst Frequency	The total number of Single Electrode Bursts in Hz divided by the analysis period.or a well, the average of the electrode burst frequencies are reported.
Burst Percentage	This is the number of spikes in a single electrode burst multiplied by 100, divided by the total number of spikes. For wells, the average of the electrode burst rate are reported.
Network Burst Frequency	The total number of network bursts divided by the analysis period in Hz.
Network Burst Duration	The average time from first spike to last spike of a network burst. Longer bursts indicate more excitement and less inhibition because it takes longer to end the burst.
Network Burst Percentage	The number of spikes in a network burst divided by the total number of spikes, multiplied by 100.
Synchrony Index	A unitless measure of synchronization between 0 and 1, with values closer to 1 indicating higher synchronization.

2.25 Pharmacological Experiment - Testing drug effects on neuronal function, including dose-response and efficacy studies.

I obtained Phenytoin Sodium from SAMJIN Pharm (Seoul, Republic of Korea) and

Lacosamide from SK Chemical (Seoul, Republic of Korea).

2.26 Quantification and Statistical Analysis - Statistical methods for analyzing experimental data, including significance testing and data visualization.

Data analysis was conducted using GraphPad Prism 9 (GraphPad Software Inc., Boston, Massachusetts, USA). The Shapiro-Wilk normality test was applied to assess whether the data followed a normal distribution. Depending on the experimental design and the type of comparison required, either an unpaired Student's t-test or one-way analysis of variance (ANOVA) was used. For ANOVA, a post hoc Bonferroni correction was applied sequentially to account for multiple comparisons.

Statistical significance was defined as a p-value less than 0.05, with the following thresholds for notation: $p < 0.05$ (*), $p < 0.01$ (**), $p < 0.001$ (***),$p < 0.0001$ (****). All data are reported as mean ± standard error of the mean (SEM), providing an accurate representation of variability. Additional statistical details, including specific p-values and test parameters, are provided in the corresponding figure legends.

This approach ensured robust statistical analysis and reliable interpretation of experimental outcomes.

3. Results

By employing Next Generation Sequencing (NGS), we successfully built a comprehensive genetic library (Figure 1) and confirmed *SCN8A* mutations in patients exhibiting developmental delays, and seizures (Table 3).

3.1 Confirmation of *SCN8A* patient genetic variants, PBMC culture, and reprogramming of iPSCs

The patient's mutation was identified as c.4871T>G in the *SCN8A* gene. This mutation led to the substitution of Isoleucine (Ile) with Serine (Ser) at position 1624 of the *SCN8A* protein (p.Ile1624Ser) (Figure 4). The mutation represented a heterozygous change in the *SCN8A* gene. The highly conserved isoleucine residue highlights the significance of this missense variant, which has not been previously reported in DEE patients or the general population.

DNA extracted from both the iPSCs and the original PBMCs was analyzed to ensure genetic consistency. STR analysis demonstrated that the iPSCs were derived from the same genetic line as the PBMCs (Figure 5A). Furthermore, Sanger sequencing confirmed that the mutation location, c.4871T>G, remained consistent in the iPSCs (Table 11).

The iPSCs were cultured for at least five passages, and karyotyping confirmed that the cells exhibited a normal chromosomal composition (46XY) (Figure 5B). STR analysis confirmed genetic identity between SCN8A patient-derived iPSCs and the corresponding patient monocytes (Figure 5C). Immunocytochemical analysis of iPSC colonies derived from the patient confirmed the expression of pluripotency markers (Figure 5D). To further assess pluripotency, iPSCs were differentiated into EBs and then into all three germ layers: ectoderm, mesoderm, and endoderm. The ectodermal markers TUJ1 and PAX6, mesodermal markers Brachyury and Alpha-Smooth Muscle Actin, and endodermal markers FOXA2 and Alpha-Fetoprotein were expressed,

confirming the ability of the *SCN8A* iPSCs to differentiate into principal cell types of all three germ layers (Figure 6, Table 13). This process successfully generated a patient-derived iPSC line with confirmed pluripotency and preserved genomic integrity.

3.2 Identification and Correction of *SCN8A* Mutation in Patient-Derived iPSCs

To introduce a heterozygous indel mutation in the *SCN8A* gene at c.4871T>G in an iPSC line derived from an *SCN8A* mutant patient (Figure 7A), prime editing technology was employed. A pegRNA was designed to target *SCN8A* specifically, incorporating the desired T>G substitution and a reverse transcriptase template. The pegRNA and a nick sgRNA (ngRNA) were cloned into a prime editing vector, encoding a Cas9 nickase-reverse transcriptase fusion protein. The sequences used for prime editing are listed in Table 14. Following prime editing, we confirmed that SCN8A c.4871T was successfully corrected to c.4871G (Figure 7B).

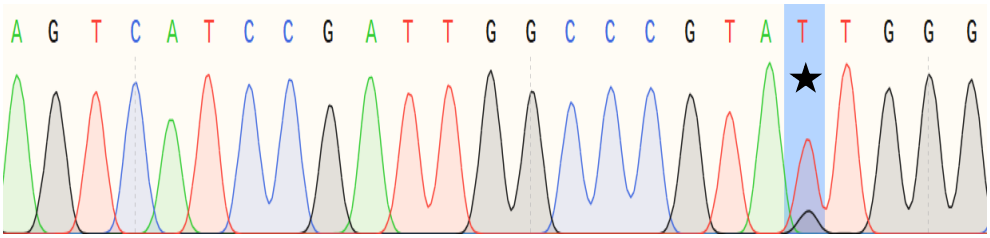

Figure 4. The voltage-gated sodium channel alpha subunit 1.6 (SCN8A) point mutation c.4871T>G (p.Ile1624Ser) identified by Sanger sequencing.

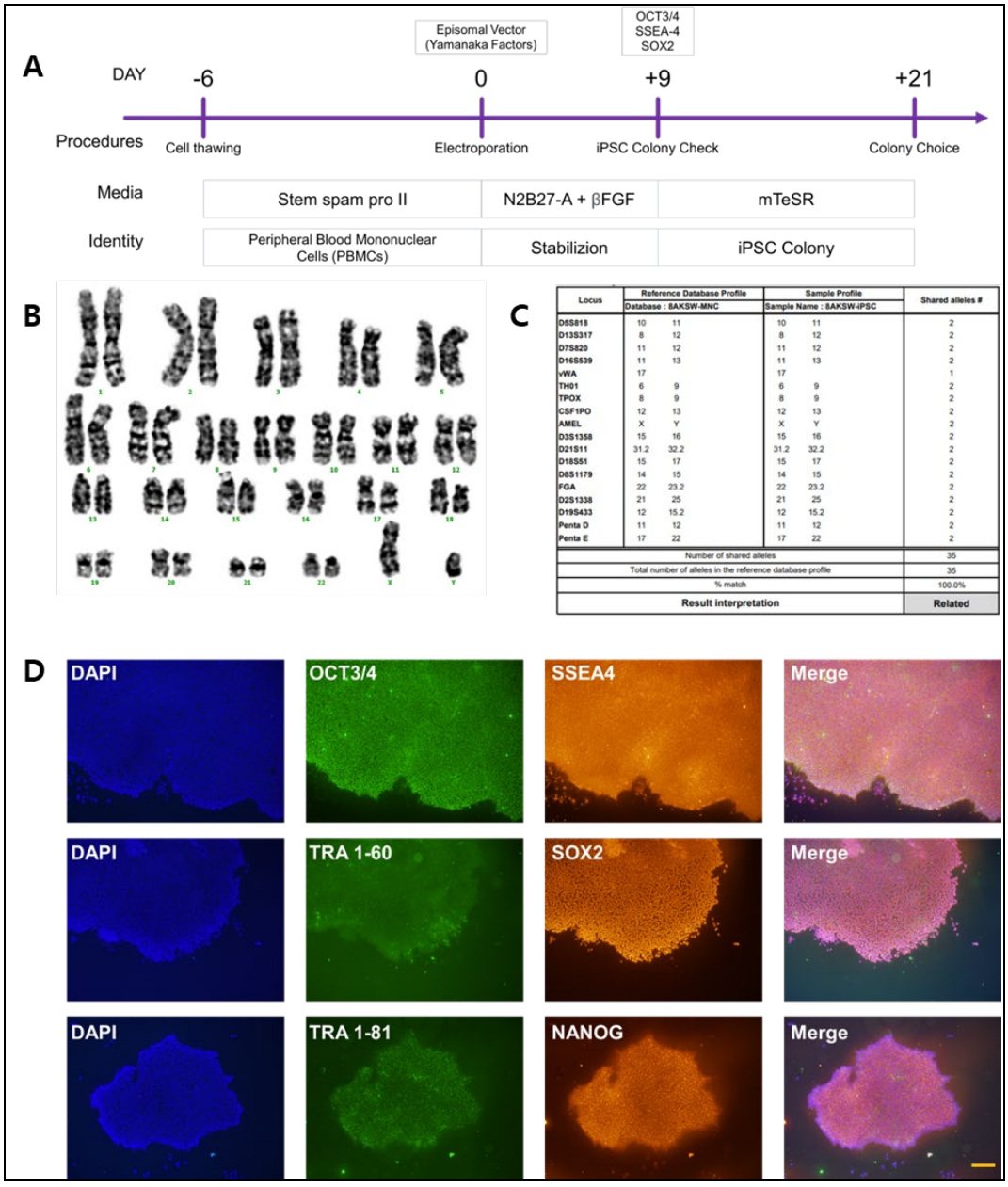

Locus	Reference Database Profile		Sample Profile		Shared alleles #
	Database : 8AKSW-MNC		Sample Name : 8AKSW-iPSC		
D5S818	10	11	10	11	2
D13S317	8	12	8	12	2
D7S820	11	12	11	12	2
D16S539	11	13	11	13	2
vWA	17		17		1
TH01	6	9	6	9	2
TPOX	8	9	8	9	2
CSF1PO	12	13	12	13	2
AMEL	X	Y	X	Y	2
D3S1358	15	16	15	16	2
D21S11	31.2	32.2	31.2	32.2	2
D18S51	15	17	15	17	2
D8S1179	14	15	14	15	2
FGA	22	23.2	22	23.2	2
D2S1338	21	25	21	25	2
D19S433	12	15.2	12	15.2	2
Penta D	11	12	11	12	2
Penta E	17	22	17	22	2
Number of shared alleles					35
Total number of alleles in the reference database profile					35
% match					100.0%
Result interpretation					**Related**

Figure 3. Confirmation of induced pluripotent stem cell identity.

(A) Establishment of patient-derived iPSCs from *SCN8A* patient monocytes. (B) Results of G-

banding analysis confirming the karyotypic stability of iPSCs. (C) Results of STR analysis comparing genes in *SCN8A* patient-derived iPSCs and *SCN8A* patient monocytes. (D) Immunocytochemistry of iPSC colonies derived from *SCN8A* patients demonstrating the expression of pluripotency markers: [OCT3/4, SSEA4], [NANOG, TRA 1-81], and [SOX2, TRA 1-60]. Scale bar = 100 μm.

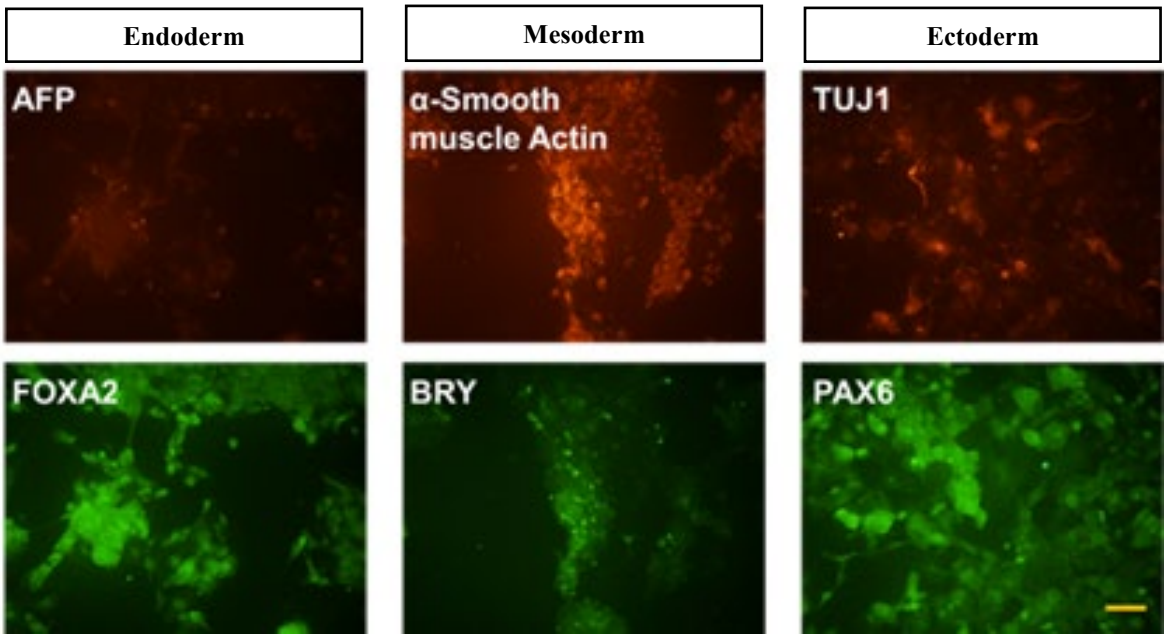

Figure 4. Differentiation of *SCN8A* patient-derived iPSCs into derivatives of three germ layers
This figure demonstrates the successful differentiation of *SCN8A* patient-derived iPSCs into the three primary germ layers: ectoderm, mesoderm, and endoderm. Immunocytochemistry analysis was conducted to verify the expression of specific markers for each germ layer. For ectoderm, TUJ1 and PAX6 were observed, indicating neural and epithelial lineage differentiation. The mesodermal lineage was confirmed through the expression of alpha-SMA and brachyury, markers

for smooth muscle and mesodermal progenitors, respectively. For endoderm, FOXA2 and AFP were expressed, highlighting differentiation into hepatic and endodermal cell types. Scale bars = 100μm.

Table 12. Antibody of iPSCs characterization

Antibody	Dilution	Company, Location, CAT No.
OCT4 Monoclonal Antibody	1:400	Invitrogen, Middlesex County, Massachusetts, United States #MA5-14845
Anti-Stage-Specific Embryonic Antigen-4 Antibody, clone MC-813-70	1:500	Merck Millipore, Burlington, Massachusetts, United States MAB4305
Anti-Nanog antibody	1:500	ABCAM, Cambridge, United Kingdom, #AB80892
Anti-TRA-1-81 Antibody, clone TRA-1-81	1:250	Merck Millipore, Burlington, Massachusetts, United States MAB4305
Anti-Sox2 Antibody	1:500	Merck Millipore, Burlington, Massachusetts, United States MAB4305
Anti-TRA-1-60 Antibody, clone TRA-1-60	1:250	Merck Millipore, Burlington, Massachusetts, United States MAB4360
Goat anti-Mouse IgG (H+L) Cross-Adsorbed Secondary Antibody, Alexa Fluor™ 568	1:500	Invitrogen, Middlesex County, Massachusetts, United States #A-11004
Goat anti-Rabbit IgG (H+L) Cross-Adsorbed Secondary Antibody, Alexa Fluor™ 488	1:500	Invitrogen, Middlesex County, Massachusetts, United States #A-11008

Table 13. Antibodies available for the three germ layers.

Antibody	Dilution	Company, Location, CAT No.
Recombinant Anti-PAX6 antibody	1:350	ABCAM, Cambridge, United Kingdom, #EPR15858
Anti-Tubulin Antibody, beta III isoform, CT, clone TU-20 (Similar to TUJ1)	1:500	Merck Millipore, Burlington, Massachusetts, United States MAB1637
Recombinant Anti-Brachyury / Bry antibody	1:1000	ABCAM, Cambridge, United Kingdom, #EPR18113
Alpha-Smooth Muscle Actin Monoclonal Antibody (1A4)	1:1000	Invitrogen, Middlesex County, Massachusetts, United States #14-9760-80
AFP Monoclonal Antibody (F1-6P2A8-P2B9A9)	1:200	Invitrogen, Middlesex County, Massachusetts, United States #MA5-14665
FOXA2 Recombinant Rabbit Monoclonal Antibody (9H5L7)	1:100	Invitrogen, Middlesex County, Massachusetts, United States #701698
Goat anti-Mouse IgG (H+L) Cross-Adsorbed Secondary Antibody, Alexa Fluor™ 568	1:500	Invitrogen, Middlesex County, Massachusetts, United States #A-11004
Goat anti-Rabbit IgG (H+L) Cross-Adsorbed Secondary Antibody, Alexa Fluor™ 488	1:500	Invitrogen, Middlesex County, Massachusetts, United States #A-11008

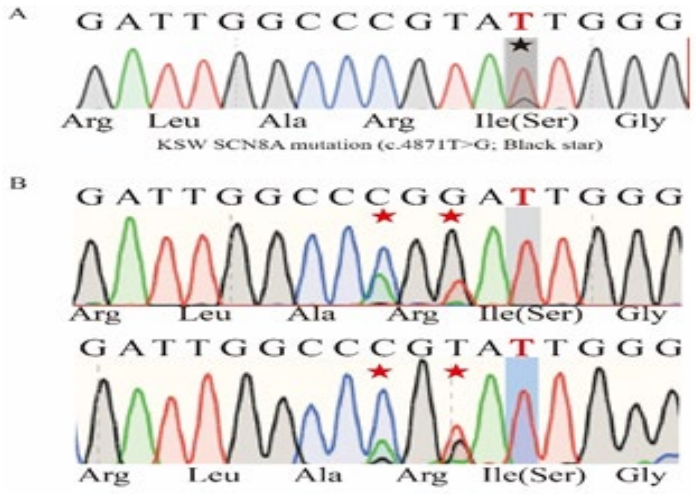

Figure 7. Results of SCN8A (c.4871 T>G) mutation correction using prime editing

(A) Confirmation of the SCN8A (c.4871 T>G) mutation. (indicated by a black star) (B) Confirmation of the correction of the SCN8A (c.4871 T>G) mutation and the introduction of a silent mutation in the PAM sequence to prevent Cas9-induced repeat cleavage (indicated by a red star)

Table 14. sgRNA, pegRNA, and nicking sgRNA sequences for plasmid construction

OligoName	Sequence	Description
sgF 32bp	CACCGACGCAAGATGCGCCCACTAGTTTTAGA	sgRNA, forward
sgR 32bp	TAGCTCTAAAACTAGTGGGCGCATCTTGCGTC	sgRNA, reverse
scaffF 64bp	GCTAGAAATAGCAAGTTAAAATAAGGCTAGTCCGTTATCAACTTGAAAAAGTGGCACCGAGTCG	Scaffold, forward (invariant)
scaffR 64bp	GCACCGACTCGGTGCCACTTTTTCAAGTTGATAACGGACTAGCCTTATTTTAACTTGCTATTTC	Scaffold, reverse (invariant)
extensF 28bp (20210216)	ATTGGCCAGGATTGGGCGCATCTT	3' extension, forward
extensR 28bp	AAAAAAGATGCGCCCAATCCTGGCCAAT	3' extension, reverse
PE3_sgF 25bp	CACCGCCTCTTCTTAGGAATGTTCC	PE3 nick sgRNA, forward
PE3_sgR 25bp	AAACGGAACATTCCTAAGAAGAGGC	PE3 nick sgRNA, reverse
PE3b_sgF 25bp	CACCGTCATCCGATTGGCCCGTATT	PE3b nick sgRNA, forward
PE3b_sgR 25bp	AAACAATACGGGCCAATCGGATGAC	PE3b nick sgRNA, reverse

3.3 Optimizing Neuronal Differentiation for *SCN8A* Patient-Derived iPSCs

Using iPSCs derived from *SCN8A* patients, neurons were generated through optimized differentiation protocols. Spontaneous differentiation is possible by altering environmental conditions, but this approach often results in heterogeneous and suboptimal differentiation into neurons specific to the Central Nervous System (CNS). To address this, a Lenti-virus-based

differentiation system was adopted, as outlined in Nature and Cell protocols.

When transcription factors ASCL1 and DLX2 were overexpressed via Lenti-Virus in iPSCs, inhibitory neurons (GABAergic neurons) were effectively generated. Similarly, the addition of NGN2 to the Lenti-Virus promoted the differentiation into excitatory neurons (Glutamatergic neurons). Conventional methods using multiple viruses caused high viral titers and inefficient selection due to the lack of unified selection markers. To address this, a redesigned Lenti-Virus system was developed, enhancing differentiation efficiency by combining transcription factors into a single virus construct (Figure 8A and 8B). This improved system significantly reduced cellular stress and streamlined the process. The redesigned lentiviral system included fluorescent markers to facilitate tracking of successful viral transduction and incorporated a unified selection marker, such as anti-puromycin, to eliminate uninfected cells. For the induction of inhibitory neurons, ASCL1 and DLX2—previously delivered via separate viral vectors—were combined into a single construct. This integration reduced the need for sequential antibiotic treatments with hygromycin and puromycin, thereby minimizing cellular stress and improving overall cell viability. Additionally, a Tet-On inducible system was implemented, enabling precise control of transcription factor expression through DOX, which enhanced the efficiency and specificity of neuronal differentiation by allowing regulated activation of key transcriptional programs (Figure 8C). To optimize viral infection efficiency, DOX (2 μg/mL) was added to the culture medium, followed by puromycin treatment for three days to remove non-infected cells. Additionally, Cytarabine (Ara-C) was introduced to suppress the proliferation of non-neuronal cells, such as fibroblasts and glial cells, ensuring a pure neuronal population. Neuronal activity and survival were further enhanced by supplementing the medium with Brain-Derived Neurotrophic Factor (BDNF), Glia-

Derived Neurotrophic Factor (GDNF), Ascorbic Acid, and dibutyryl cyclic-AMP (dbcAMP). Forskolin, a diterpene compound, was added to increase intracellular cAMP levels, promoting synaptic efficiency and neuronal viability.

After 12 days, differentiated neurons were co-cultured with astrocytes to mimic the cortical brain environment. This co-culture system provides critical support for neuronal maturation, as astrocytes secrete factors essential for synaptic development and neuronal health. While Astrocyte-Conditioned Media (ACM) has been explored as an alternative, direct co-culture was selected to ensure a more physiologically relevant environment. Neurons and astrocytes were co-cultured at a 1:1 ratio to establish a balanced system that supports the growth and functionality of both cell types. Astrocytes were derived from primary cultures of postnatal day 0 mouse brains (Figure 9).

Electrophysiological properties of the neurons were assessed using MEA technology. For MEA experiments, GABAergic and Glutamatergic neurons were co-cultured in a 3:7 ratio, reflecting the forebrain cortical environment. This configuration allowed for a functional analysis of neuronal activity in a controlled setting. Individual neurons were also grown on slide glass for mRNA extraction and characterization. These methods enabled precise measurement of neuronal differentiation and synaptic activity (Figure 9).

The redesigned Lenti-Virus system and optimized differentiation timeline significantly improved the efficiency and accuracy of neuronal differentiation from *SCN8A* patient-derived iPSCs.

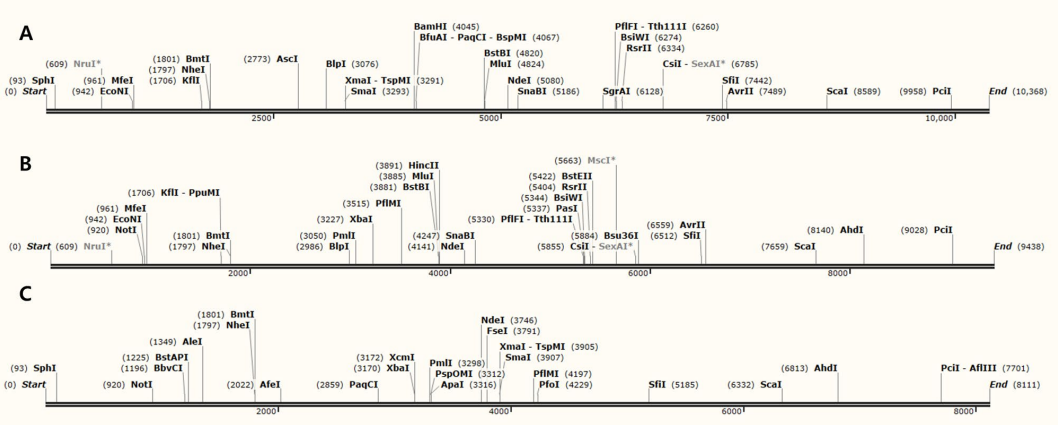

Figure 8. Lenti virus design. (A) Tet-on-based Lenti-virus specialized for differentiation into GABAergic neurons includes both hASCL1 and hDLX2 transcription factors. It is equipped with mCherry and Anti-Puro as selection markers to enhance the efficiency of viral infection and ensure proper cell selection. This design streamlines the differentiation process, enabling effective generation of GABAergic neurons. (B) Tet-on-based Lenti-virus designed for differentiation into Glutamatergic neurons contains the NGN2 transcription factor, along with selection markers eGFP and Anti-Puro. The inclusion of these features improves the efficiency of the Lenti-virus system, facilitating the differentiation into functional Glutamatergic neurons. (C) Both (A) and (B) utilize Tet-On systems, requiring the presence of rtTA to activate the Lenti-virus under Doxycycline (DOX) induction. The rtTA construct was redesigned to ensure proper activation of the viral system, allowing for controlled differentiation into GABAergic and glutamatergic neurons.

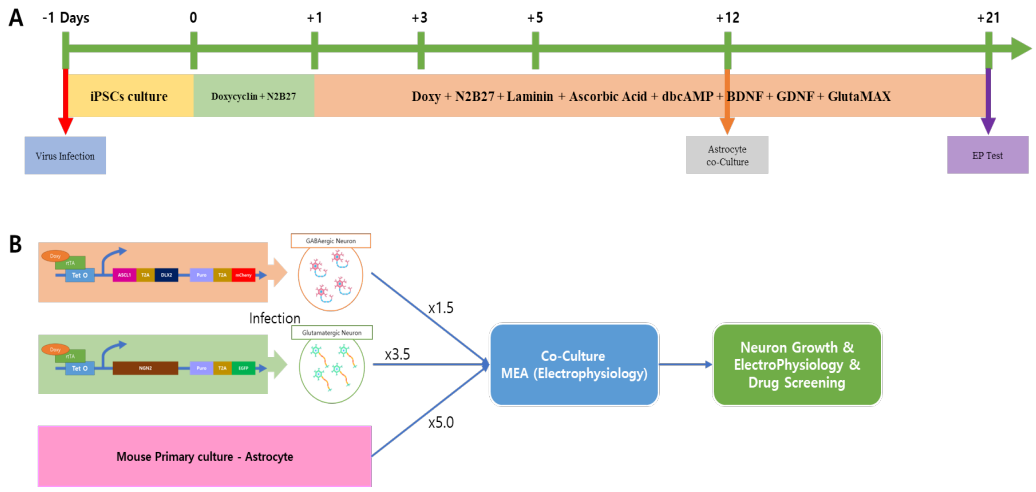

Figure 9. Illustration of neuronal differentiation timeline and application scheme.

(A) The timeline depicts the process of differentiation of iPSCs into neurons. Key stages include the initial culture phase, transcription factor induction via Tet-On-based Lenti-virus, and neuronal maturation phases supported by essential supplements like BDNF, GDNF, and dbcAMP. (B) Application plan for differentiated neurons, including co-culture with astrocytes, electrophysiological studies, and drug screening for SCN8A-related disorders.

3.4 Electrophysiological Activity of Neurons Derived from SCN8A Patient iPSCs on a MEA

To investigate functional differences between SCN8A patient-derived neurons and genetically corrected neurons, electrophysiological analyses were conducted using MEA technology. Recordings began three weeks after differentiation, allowing sufficient time for early neuronal maturation. The neuronal composition was adjusted to mimic the human forebrain cortex, with GABAergic neurons and glutamatergic neurons co-cultured in a 3:7 ratio. Astrocytes were included at a 1:1 ratio with total neurons to create a physiologically relevant microenvironment. Dox was administered to induce transcription factor activation, and the

cultures were maintained for three to six weeks to allow sufficient neuronal and network maturation.

Electrophysiological activity was assessed using heat maps, which revealed distinct firing patterns in neurons derived from SCN8A patients. At three weeks post-differentiation, these neurons exhibited elevated activity, as indicated by densely active regions on the heat map (Figure 10A). Fluorescence imaging confirmed the proper distribution of neurons and astrocytes on the MEA, along with appropriate cell adhesion and neurite extension (Figure 10B). This hyperactivity was sustained and became more pronounced over time. By six weeks, the neurons displayed widespread and robust activity (Figure 10C). MEA recordings further identified spontaneous network bursts, characterized by frequent bursts and excessive firing, indicative of heightened neuronal excitability (Figure 10D).

Patient-derived neurons exhibited significantly elevated firing rates, with an approximately 11-fold increase from week 3 to week 6 (Figure 11A). At three weeks, the mean firing rate (MFR) was 1.117 Hz ± 0.071 Hz (SEM), which increased to 6.324 Hz ± 0.340 Hz at four weeks, 10.903 Hz ± 0.511 Hz at five weeks, and 11.498 Hz ± 0.636 Hz at six weeks.

The burst frequency was calculated at the standard level. It showed similar values across weeks: 0.071 Hz ± 0.003 Hz at 3 weeks, 0.050 Hz ± 0.003 Hz at 4 weeks, 0.048 Hz ± 0.003 Hz at 5 weeks, and 0.061 Hz ± 0.007 Hz at 6 weeks (Figure 11B). Burst percentage was 25.346 Hz ± 1.537 Hz at 3 weeks, increasing significantly to 77.631 Hz ± 1.656 Hz at 4 weeks and peaking at 85.985 Hz ± 1.379 Hz at 5 weeks. However, at 6 weeks, it slightly declined to 81.316 Hz ± 2.707 Hz. This trend may be associated with the viability of the neurons, as a notable tendency for glutamatergic neurons to lose viability was observed after 5 to 6 weeks (Figure 11C).

Network bursts, defined as spikes that are nearly synchronized across multiple electrodes, progressively increased over time. The network burst frequency was 0.081 Hz ± 0.006 Hz at 3 weeks, 0.089 Hz ± 0.003 Hz at 4 weeks, 0.104 Hz ± 0.005 Hz at 5 weeks, and 0.132 Hz ± 0.007 Hz at 6 weeks (Figure 11D). The Network Burst Percentage showed a significant difference starting at week 4. Notably, it was approximately half at week 3, with a value of 55.023 ± 3.848. From week 4, it increased dramatically to 93.150 ± 0.493, reaching 94.842 ± 0.338 at week 5, and slightly decreasing to 93.184 ± 0.819 at week 6 (Figure 11E). Synchronization analysis revealed that mutant neurons exhibited higher synchronization levels at earlier stages, indicative of excessive network coupling.

Synchrony was quantified using normalized cross-correlation analyses, which accounted for spike timing and frequency across electrode pairs. For the Synchrony Index, the value was relatively low at 0.091 ± 0.007 in week 3. However, the mean value increased as the weeks progressed, reaching 0.587 ± 0.020 in week 4, 0.742 ± 0.017 in week 5, and slightly decreasing to 0.712 ± 0.028 in week 6. (Figure 11F).

These neurons exhibited a steady increase in firing rates, burst frequencies, and levels of synchrony over time. Such findings align with the epileptic phenotype associated with SCN8A mutations, where excitatory neuronal activity became more pronounced over time. Differences in neuronal activity became more pronounced over time, with patient neurons showing a substantial increase in activity as they transitioned from week 3 to week 4. However, a slight decrease in activity was observed at week 6. (Figures 11). These findings underscore the critical role of *SCN8A* in regulating neuronal network dynamics.

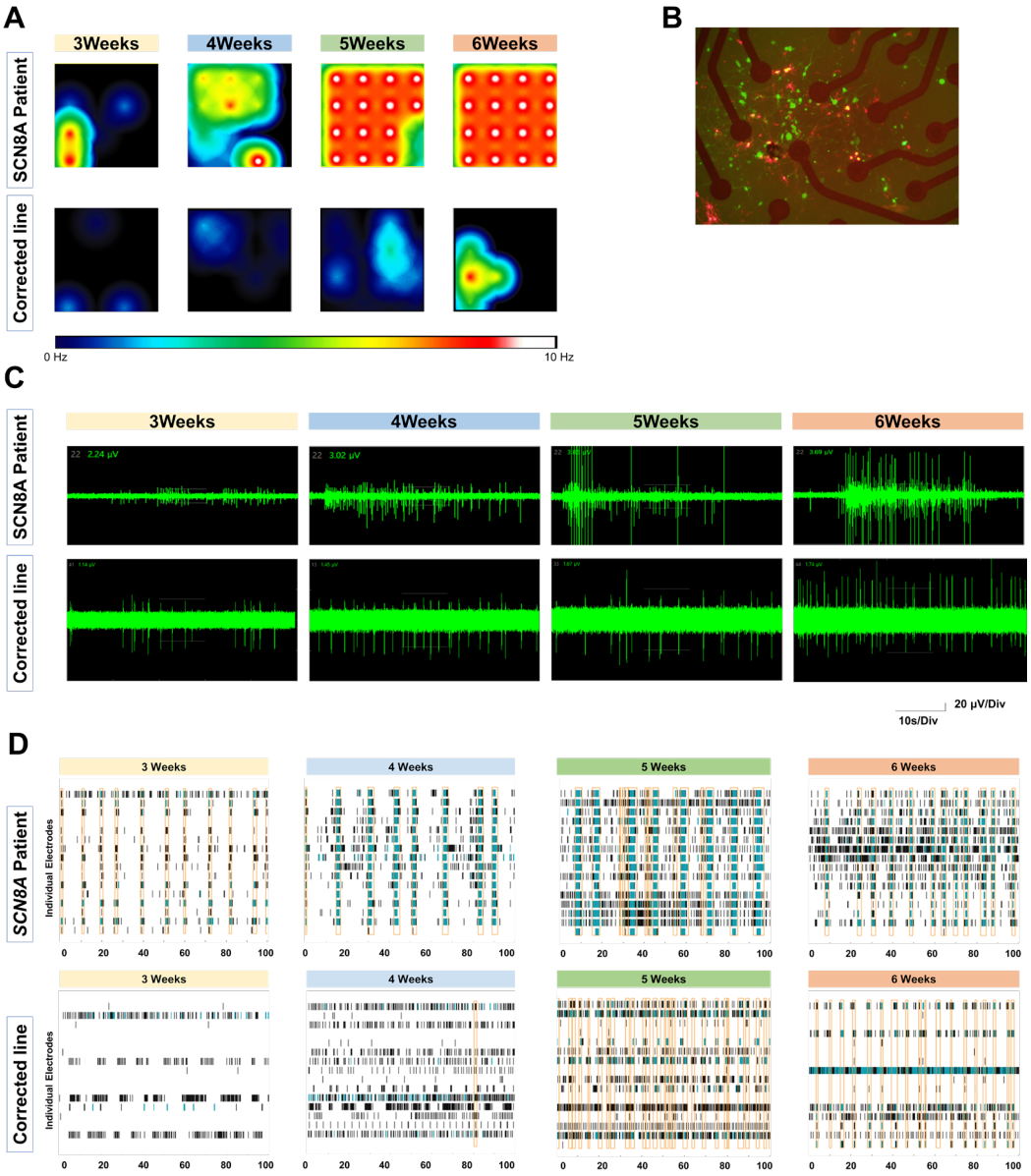

Figure 10. Suppressed network excitability demonstrated by MEA recordings of hiPSC-derived neurons with isogenic correction of the c.4871T>G mutation.

(A) Heat map displaying neuronal firing activity across development, where firing frequency

intensity is visually represented by a color spectrum. Cool tones (blue, green) indicate low firing frequency, and the absence of warm tones (red, white) reflects reduced excitability across the electrode array. Each colored circle denotes an active electrode, and limited activation is observed over time compared to the patient line. (B) Well-plated MEA with hiPSC-derived neurons, where fluorescence labeling distinguishes neuronal subtypes: RFP (red) marks GABAergic neurons, while eGFP (green) labels Glutamatergic neurons. (Scale bar = 100 μm) (C) Representative spike traces from corrected neuron cultures across four time points. Each spike represents a spontaneous activity event. Notably, spike amplitude and frequency remain relatively stable and low, indicating restored membrane excitability and absence of aberrant bursting. (D) Raster plots showing temporal spike patterns across electrodes over 100 seconds. Spike events are sparsely distributed with no evidence of synchronized bursts, demonstrating a normalized network activity profile following gene correction.

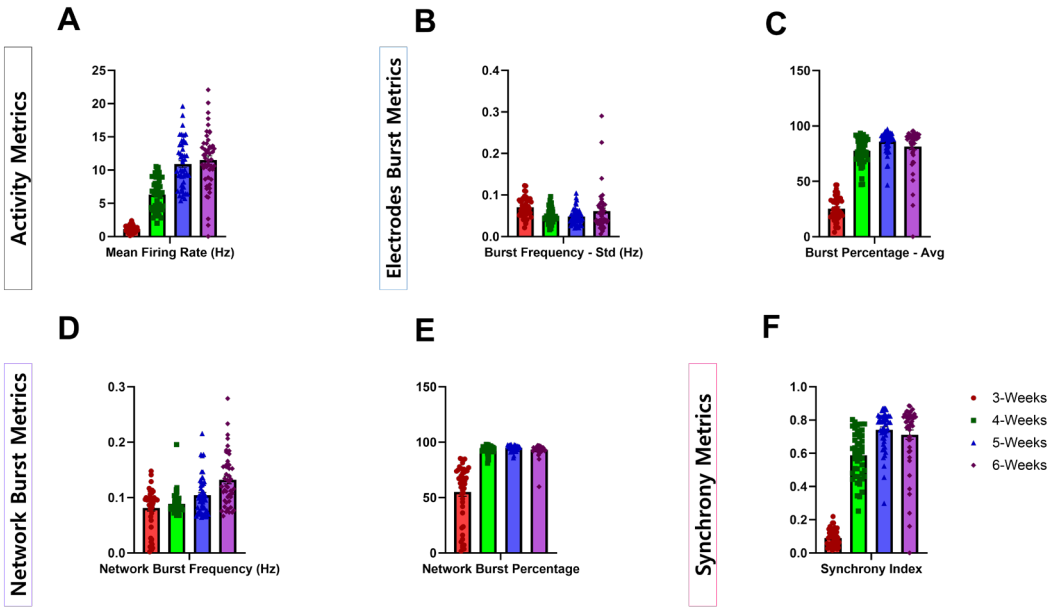

Figure 11. Measurement of *SCN8A* action potentials using MEA.

(A) Mean firing rate (MFR) : MFR increased significantly from 1.117 Hz ± 0.071 (week 3) to 11.498 Hz ± 0.636 (week 6), showing an ~11-fold rise. (B) Burst frequency : Burst frequency remained stable, with values ranging from 0.071 Hz ± 0.003 (week 3) to 0.061 Hz ± 0.007 (week 6). (C) Burst percentage : Burst percentage increased from 25.346 Hz ± 1.537 (week 3) to 85.985 Hz ± 1.379 (week 5), with a slight decline at week 6. (D) Network burst frequency : Network bursts increased from 0.081 Hz ± 0.006 (week 3) to 0.132 Hz ± 0.007 (week 6). (F) Synchrony index : Synchrony rose from 0.091 ± 0.007 (week 3) to 0.742 ± 0.017 (week 5), with a slight decrease at week 6.

3.5 Electrophysiological Characterization of *SCN8A* Patient-Derived Neurons and Their Genetically Corrected Controls

To investigate the functional characteristics of *SCN8A* patient-derived neurons in comparison with genetically corrected neurons, electrophysiological analyses were conducted using MEA technology. Neurons were analyzed starting at three weeks post-differentiation. Genetically corrected neuron cultures were also maintained for three to six weeks to allow for sufficient neuronal and network maturation. Corrected neurons exhibited markedly reduced network excitability and maintained firing stability throughout all stages of maturation. At week 3, heatmap analysis showed sparse and spatially confined neuronal firing, with only a few electrodes displaying low-frequency spikes in cool tones (blue to green). This pattern remained consistent at week 4, with only slight increases in localized activity and no expansion across the electrode array. In contrast to patient-derived neurons, which showed widespread network activation by week 5, corrected neurons continued to exhibit low firing levels restricted to isolated or small clusters of electrodes. By week 6, although moderate increases in activity were observed in certain regions, overall firing remained spatially restricted and low in intensity, suggesting that gene correction effectively suppressed hyperexcitability (Figure 10A).

Spike trace recordings further supported the suppression of aberrant firing in corrected neurons. At week 3, only infrequent and low-amplitude spontaneous activity was observed, with no evidence of high-frequency spike clusters. As differentiation progressed, the corrected neurons showed mild increases in spike amplitude and frequency, particularly at weeks 5 and 6, but the activity remained well-regulated and clearly distinct from the hyperactive bursting seen in patient neurons. Even at later stages, electrophysiological traces maintained a stable baseline membrane potential, with few synchronized spikes and no prolonged burst episodes. These findings strongly

suggest that gene correction effectively reduced the membrane hyperexcitability associated with the *SCN8A* mutation (Figure 10C).

Raster plot analysis further illustrated the temporal and spatial control of network activity in corrected neurons. At week 3, spikes were sparsely distributed across the electrode grid with minimal vertical alignment, indicating an absence of synchronous firing. Although firing density increased slightly by week 4, events remained temporally dispersed and largely asynchronous. At week 5, a modest increase in spike activity across more electrodes was observed, yet there was no emergence of strong clustering or synchrony. Even by week 6, although firing density had grown, large-scale synchronized network bursts-characteristic of patient neurons-did not appear. The absence of dense vertical spike bands at all time points supports the notion that firing patterns in the corrected neurons are physiologically regulated. (Figure 10D).

Corrected neurons demonstrated significantly suppressed excitability and normalized network behavior over time, contrasting the hyperactive patterns observed in patient-derived neurons. At week 3, the mean firing rate (MFR) of the corrected neurons was 0.288 Hz ± 0.035 Hz (SEM), reflecting a relatively low baseline activity typical of early-stage neuronal cultures. By week 4, the MFR rose modestly to 1.058 Hz ± 0.139 Hz, and further increased to a peak of 1.403 Hz ± 0.196 Hz at week 5. However, at week 6, a slight reduction in firing activity was observed, with the MFR measuring 1.114 Hz ± 0.156 Hz. This overall pattern shows a limited increase in intrinsic neuronal firing over the differentiation period, which remained within physiological levels and did not exhibit the pathological overactivation characteristic of SCN8A-mutant neurons. Notably, while the corrected neurons followed a general trend of maturation, they did not exhibit the exponential escalation in firing rates seen in patient neurons, suggesting a successful normalization of action potential activity

through genetic correction (Figure 12A). Burst frequency, calculated as the average number of single-electrode burst events per second within each well, demonstrated a distinct temporal progression in corrected neurons. At week 3, the burst frequency was 0.038 Hz ± 0.009 Hz, indicating sparse and infrequent burst activity in the early stages of culture development. This frequency increased steadily to 0.118 Hz ± 0.017 Hz by week 4 and reached a peak of 0.158 Hz ± 0.020 Hz at week 5, reflecting the ongoing maturation of intrinsic neuronal bursting. Interestingly, a slight reduction to 0.120 Hz ± 0.020 Hz was observed at week 6, suggesting that while network excitability increased with differentiation, it stabilized rather than escalating pathologically. The absence of sharp or erratic increases in burst frequency reinforces the interpretation that the corrected neurons maintain homeostatic control over their firing patterns across time (Figure 12B). Further evidence of normalized activity in corrected neurons was seen in the burst percentage, which quantifies the proportion of spikes occurring within burst events. The corrected neurons exhibited low burst participation early in development, beginning with a value of 2.933% ± 0.727% at week 3. By week 4, the burst percentage rose to 8.183% ± 1.124%, and then peaked at 11.594% ± 1.470% at week 5, consistent with a modest increase in synchronous activity as the network matured. However, this was followed by a slight decline to 9.998% ± 1.693% at week 6. Compared to the significantly higher burst percentages observed in patient neurons—often exceeding 80%—these results demonstrate that the corrected neurons remained largely resistant to developing abnormal burst dominance. The restricted increase in burst percentage, even at later time points, reflects a healthier, more regulated pattern of neuronal network activity (Figure 12C).

Network bursts, defined as large-scale, near-synchronous spike events occurring across multiple electrodes, were largely absent at early stages of corrected neuron development. At week 3, the network burst frequency was virtually negligible at 0.0002 Hz ± 0.0002 Hz, underscoring the low level of coordinated network activity at this time point. By week 4, the network burst

frequency increased to 0.057 Hz ± 0.014 Hz and further rose to 0.115 Hz ± 0.021 Hz at week 5, aligning with the gradual formation of inter-neuronal connections and maturing synaptic integration. A modest reduction to 0.080 Hz ± 0.016 Hz was recorded at week 6. This temporal pattern reflects controlled development of network-wide burst activity, which differs markedly from the rapid and excessive synchronization observed in patient neurons. The relatively moderate frequency of network bursts in corrected neurons supports the conclusion that pathological hyperexcitability was effectively attenuated following genetic correction (Figure 12D).

The Network Burst Percentage—a measure of how much of the total activity occurs within these synchronized network bursts—showed a similar restrained progression. Corrected neurons began with a very low value of 0.093% ± 0.071% at week 3, consistent with their limited initial network engagement. A significant increase occurred at week 4, with the value rising to 14.333% ± 3.612%, suggesting the onset of coordinated synaptic communication. This trend continued into week 5, reaching a peak of 25.981% ± 4.598%, before a mild decline to 21.008% ± 4.050% at week 6. Although network burst participation increased over time, it remained at a much lower level compared to patient neurons, where values exceeded 90% from week 4 onward. The more moderate increase in network burst percentage in corrected neurons reflects a healthier network configuration, in which neurons engage in periodic synchrony without falling into sustained pathological burst states (Figure 12E).

Synchronization analysis revealed that spike timing and synchrony across electrodes in corrected neurons remained relatively low and stable throughout the differentiation period. At week 3, the synchrony index was 0.054 ± 0.022, indicating minimal early-stage coupling between neurons. Although a gradual increase was

observed—rising to 0.072 ± 0.011 by week 6—the corrected neurons never approached the excessive synchrony levels found in patient neurons. This sustained suppression of network-wide synchrony suggests effective normalization of connectivity and firing patterns, likely attributable to restoration of proper sodium channel function via correction of the SCN8A mutation. The absence of pronounced peaks or variability in the synchrony index further confirms the functional stability of the corrected neuronal networks (Figure 12F).

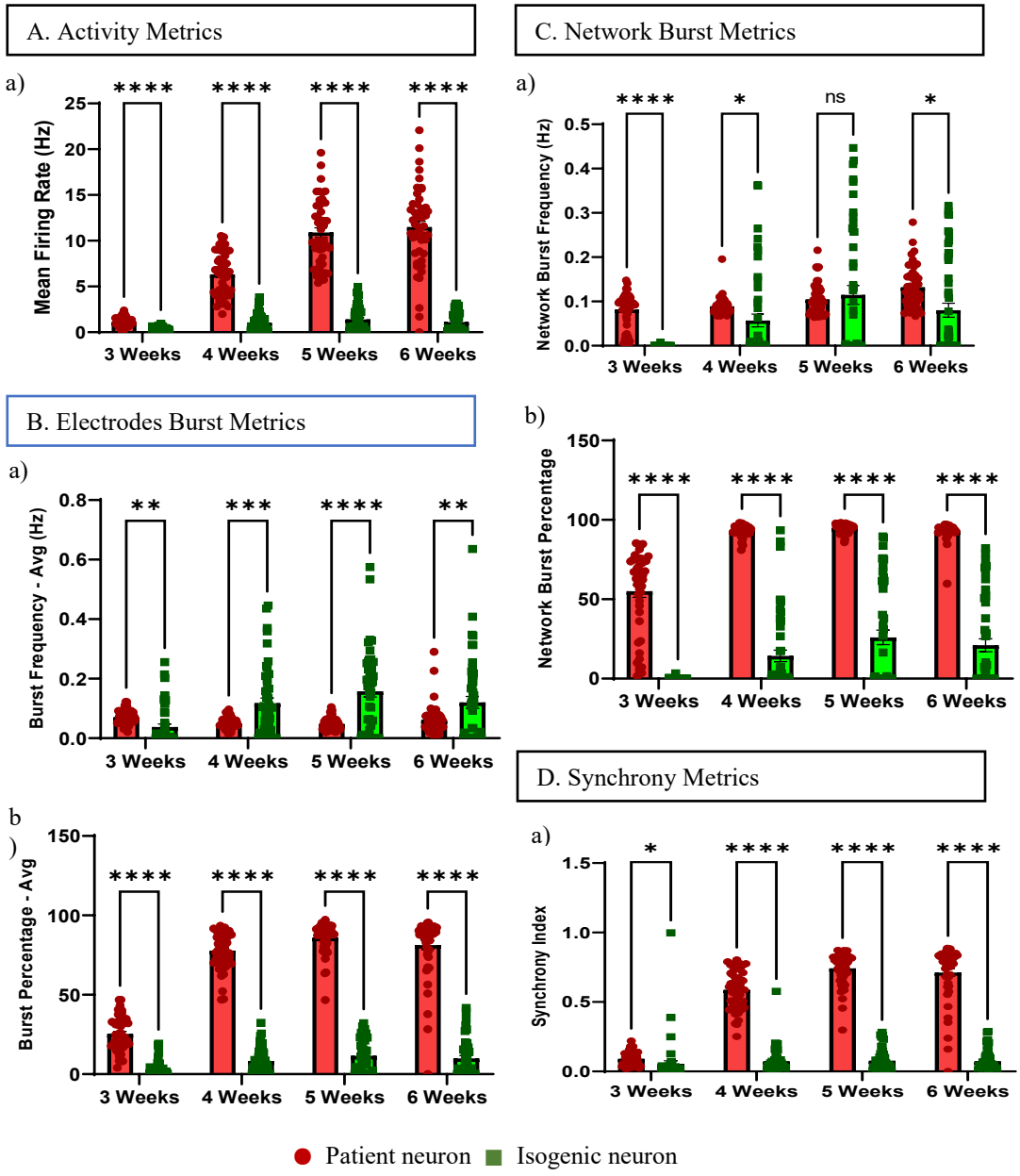

Figure 12. Measurement of *SCN8A* action potentials using MEA. A. Activity metrics. a) Mean firing rate (MFR): In patient neurons, MFR increased significantly from 1.117 Hz ± 0.071 (week 3) to 11.498 Hz ± 0.636 (week 6), showing an approximately 11-fold rise. In contrast, corrected

neurons exhibited only a mild increase from 0.288 Hz ± 0.035 (week 3) to 1.403 Hz ± 0.196 (week 5), followed by a slight decline to 1.114 Hz ± 0.156 in week 6. B. Electrodes burst metrics. a) Burst frequency: Patient neurons maintained relatively stable burst frequency, ranging from 0.071 Hz ± 0.003 (week 3) to 0.061 Hz ± 0.007 (week 6). Corrected neurons, however, showed a marked increase from 0.038 Hz ± 0.009 (week 3) to 0.158 Hz ± 0.020 (week 5), then slightly declined to 0.120 Hz ± 0.020 in week 6. b) Burst Percentage: Burst percentage in patient neurons surged from 25.346% ± 1.537 (week 3) to a peak of 85.985% ± 1.379 (week 5), with a minor decrease to 81.316% ± 2.707 at week 6. Meanwhile, corrected neurons exhibited significantly lower burst activity, increasing from 2.933% ± 0.727 (week 3) to 11.594% ± 1.470 (week 5), then decreasing slightly to 9.998% ± 1.693 in week 6. C. Network bust metrics. a) Network burst frequency: Patient neurons showed a gradual increase in network bursting from 0.081 Hz ± 0.006 (week 3) to 0.132 Hz ± 0.007 (week 6). Corrected neurons also increased over time from near-zero levels (0.0002 Hz ± 0.0002 at week 3) to 0.115 Hz ± 0.021 in week 5, followed by a decrease to 0.080 Hz ± 0.016 in week 6.b) Network burst percentage: In patient neurons, network burst percentage was consistently high, reaching over 93% from week 4 onward. In contrast, corrected neurons remained significantly lower, starting at 0.093% ± 0.071 (week 3) and reaching 25.981% ± 4.598 by week 5, then decreasing to 21.008% ± 4.050 in week 6. D. Synchrony metrics. a) Synchrony index: Patient neurons exhibited a steep increase in synchrony, from 0.091 ± 0.007 (week 3) to 0.742 ± 0.017 (week 5), with a slight decrease to 0.712 ± 0.028 by week 6. Corrected neurons showed low and stable synchrony levels throughout, ranging from 0.054 ± 0.022 (week 3) to 0.077 ± 0.011 (week 5), followed by 0.072 ± 0.011 in week 6.

3.6 Comparative Evaluation of Treatment Efficacy in *SCN8A*-Related Epilepsy

The treatment of seizure disorders should primarily target the underlying condition. While the selection of anti-seizure medications (ASMs) for seizure control has been based on seizure type, advances in genetics have led to the identification of ASMs that are tailored to the functional characteristics of specific gene variants. In SCN8A-related epilepsy, neuronal hyperexcitability is a hallmark feature, and sodium channel blockers are presumed to be effective based on this pathophysiology; therefore, they are recommended as a first-line treatment option. Phenytoin and lacosamide are representative ASMs that act by inhibiting sodium channels, with distinct mechanisms of action: phenytoin primarily enhances fast inactivation, whereas lacosamide selectively promotes slow inactivation of sodium channels. The effects of these two ASMs on mutant neurons were analyzed using MEA recordings.

To evaluate the effects of the drugs based on the electrophysiological activity of neurons using MEA recordings, we selected four items: activity metrics (firing level), electrode burst metrics (burst level), network burst metrics (network burst), and synchrony metrics (Figures 13). This represents the electrophysiological data observable at the neuronal level. I used 0 μM of dimethyl sulfoxide (DMSO) before applying the drugs, and the same amount of medium was used for all drugs per concentration (1/1000 of the concentration). DMSO also served as the solvent for the compounds. The results were computed by dividing the values acquired after 10 minutes of drug administration by the baseline values collected before drug treatment (0 μM DMSO).

The effect of phenytoin was significant, exhibiting concentration-dependent changes 10 minutes after drug administration. Among the activity metrics, the firing rate (Hz) decreased with increasing phenytoin concentration, with all p-values below 0.0001 (Figures 13A1).

Burst metrics (burst frequency and burst percentage) showed no statistically significant differences before and after drug treatment. Burst patterns remained largely unchanged across

concentrations (Figures 13B1 and C1), suggesting that the spike-to-burst pattern was preserved.

No statistically significant differences were observed in the network burst metrics, including network burst frequency and duration. Although network burst duration showed a tendency to decrease in a concentration-dependent manner, the change was not statistically significant (Figure 13D1 and E1).

Regarding synchrony metrics, the synchrony index showed statistically significant differences only at the highest phenytoin concentration (50 μM) (Figure 13F1). Burst activity, network burst activity, and synchrony are key features associated with seizure generation; therefore, the persistence of these patterns following drug treatment suggests that the neurons remained seizure-prone.

Lacosamide also showed a concentration-dependent decrease in firing rate (Hz) (Figure 13A2). It demonstrated greater effectiveness in certain parameters compared to phenytoin. Burst frequency showed a statistically significant reduction following lacosamide treatment (Figure 13B2). In network burst activity, network burst duration was significantly reduced at concentrations of 1, 20, and 40 μM (Figure 13E2), whereas phenytoin showed significant changes only at the highest concentration. However, there were also parameters in which lacosamide was less effective than phenytoin. The synchrony index showed no statistically significant differences across concentrations following lacosamide treatment (Figure 13F2).

Overall, phenytoin treatment showed a concentration-dependent decrease in network burst duration, although the reduction was only statistically significant at highest concentration (50 μM). Lacosamide exhibited statistically significant changes in burst frequency and was more effective in reducing network burst duration across a broader concentration range compared to phenytoin. Significant changes in the synchrony index were observed only with phenytoin at the highest concentrations (Figure 13).

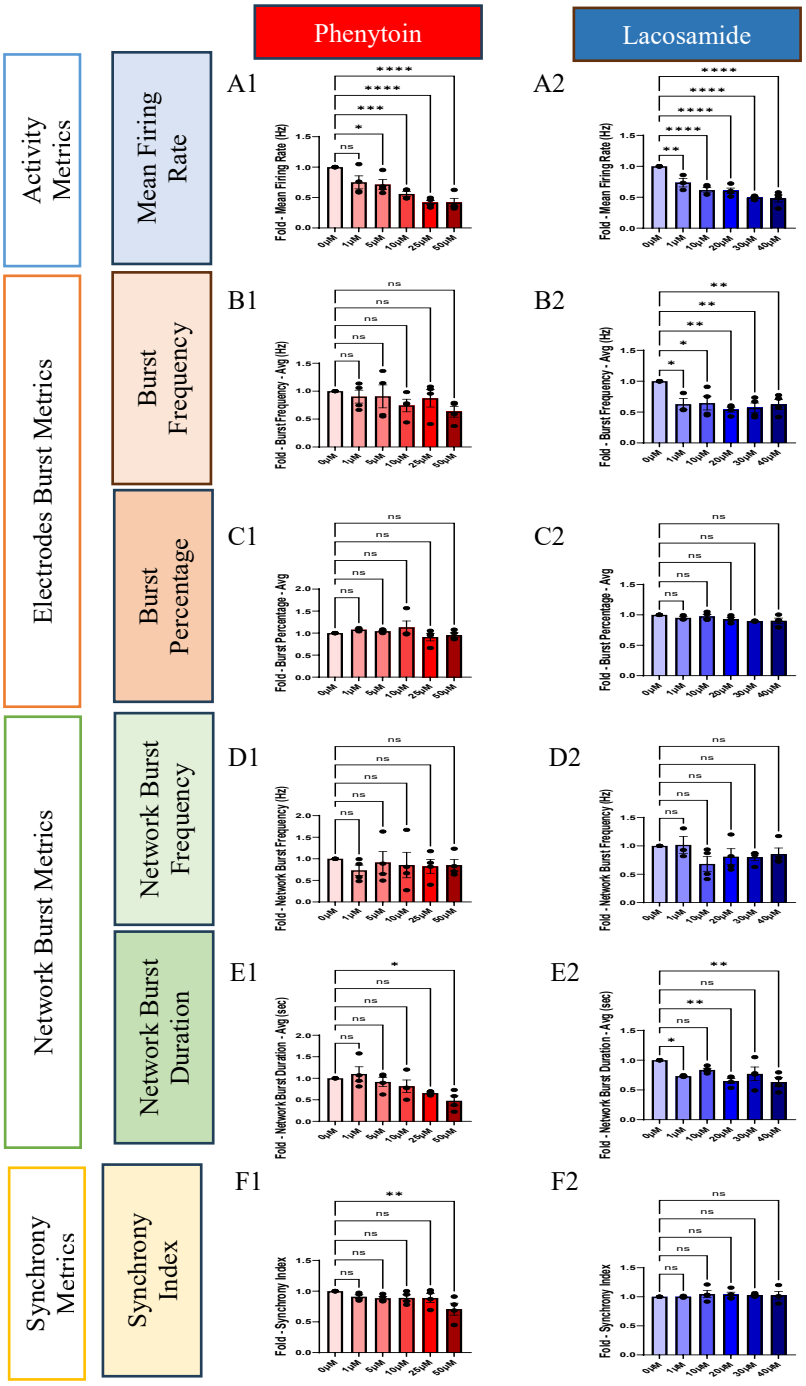

Figure 13. Response of *SCN8A* patient-derived neurons to phenytoin and lacosamide
(A1, B1, C1, D1, E1, F1) Phenytoin. (A2, B2, C2, D2, E2, F2) Lacosamide. (A1 – A2) Mean firing rate (Hz). (B1 – B2) Burst frequency – average (Hz). (C1 – C2) Burst percentage – average. (D1 – D2) Network burst frequency (Hz). (E1 – E2) Network burst duration – average (seconds). (F1 – F2) Synchrony index. N = 4, *:p≤0.05, **:p≤0.01, ***:p≤0.001, ****: p≤0.0001

3.7 Electrophysiological Response of Genetically Corrected *SCN8A* Neurons to Phenytoin and Lacosamide

The effects of phenytoin and lacosamide on corrected neurons were analyzed using the same approach as that applied to mutant neurons (Figure 14A1). Unlike in the mutant neurons, phenytoin did not induce a statistically significant change in firing rate. However, burst frequency was significantly reduced at high concentrations (Figure 14B1), and both network burst frequency and duration showed significant reductions even at low concentrations, with more pronounced effects at higher concentrations (Figure 14 D1 and E1). The Synchrony Index did not show statistically significant changes at any concentration (Figure 14 F1).

Lacosamide treatment resulted in a significant reduction in firing rate (Figure 14 A2). Unlike in mutant neurons, a statistically significant decrease was also observed in burst percentage (Figure 14 C2). In contrast to the mutant neurons, network burst frequency and duration were significantly reduced starting from low concentrations (Figure 14 D2 and E2). The Synchrony Index did not show significant changes at any concentration (Figure 14 F3).

For the both ASMs, the parameters that exhibited significant effects showed a more marked reduction in activity at higher concentrations compared to the mutant neuron line.

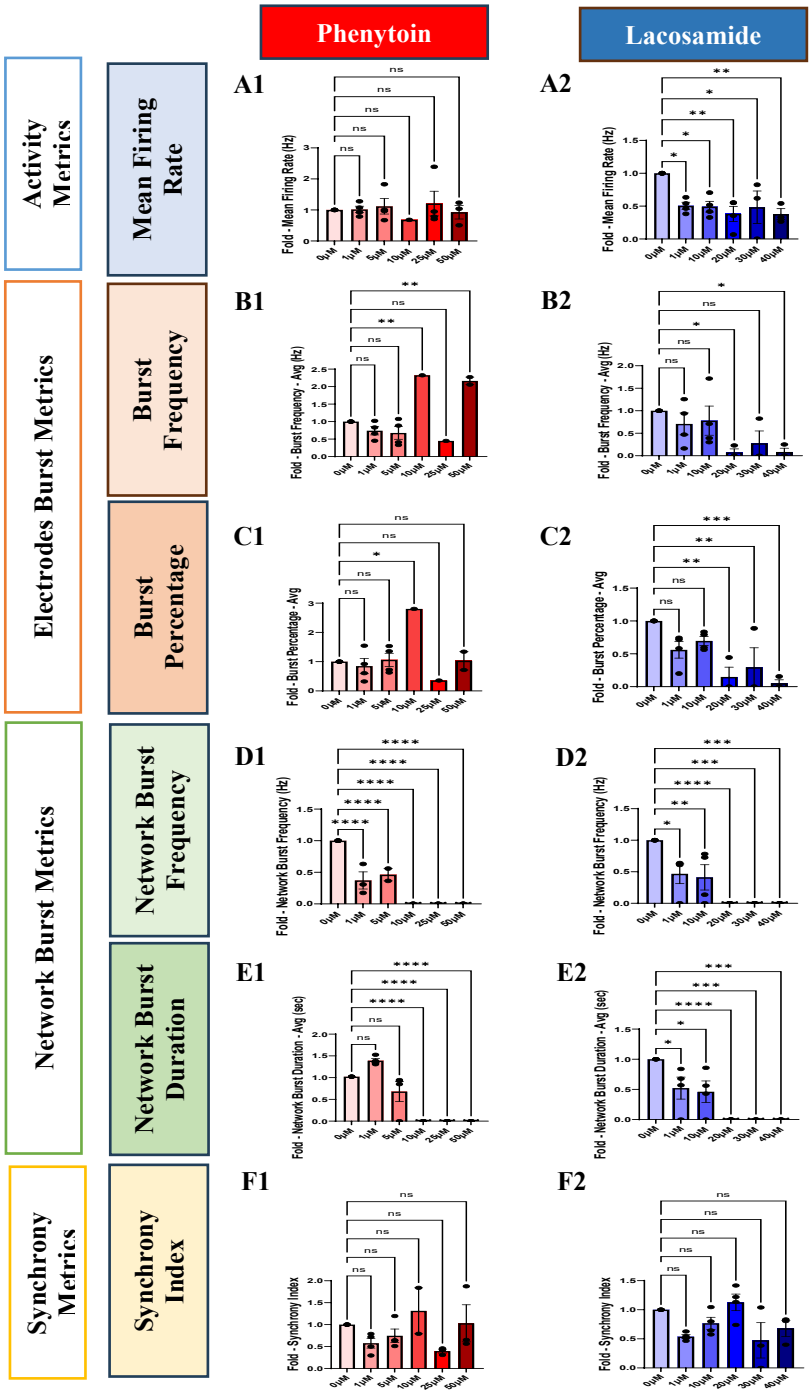

Figure 14. Response of corrected *SCN8A* patient-derived neurons to phenytoin-Na and lacosamide. (A1, B1, C1, D1, E1, F1) Phenytoin. (A2, B2, C2, D2, E2, F2) Lacosamide. (A1 – A2) Mean firing rate (Hz). (B1 – B2) Burst frequency - average (Hz). (C1 – C2) Burst percentage – average. (D1 – D2) Network burst frequency (Hz). (E1 – E2) Network burst duration - average (seconds). (F1 – F2) Synchrony index. N = 2, *:p≤0.05, **:p≤0.01, ***:p≤0.001, ****: p≤0.0001

4. Discussion

To investigate the pathological mechanisms underlying SCN8A-related disorders, patient-derived iPSCs were generated and differentiated into neurons that mimic brain-like environments. Pharmacological assays using these neuronal models enabled the evaluation of potential therapeutic strategies. In parallel, prime editing was applied to correct the SCN8A mutation, generating isogenic lines that were directly compared with the unedited patient-derived neurons. This comparison revealed distinct neuronal dysfunctions and contributed to a clearer understanding of the underlying disease mechanisms.

While pathogenic mutations may arise within the same gene or locus, the clinical severity and epileptic phenotypes can vary significantly depending on the specific mutation type and other modifying factors. Thus, disease modeling is critical for elucidating the in vivo functions of these causative genes [Du et al., 2015]. Traditional animal models, including mice and zebrafish, often fall short of replicating human-specific pathophysiology. In contrast, iPSCs retain the patient's genetic background and enable the generation of isogenic controls, offering a more accurate and personalized platform for disease modeling. Beyond their utility in recapitulating disease mechanisms, iPSCs hold significant promise in neuroscience research. When differentiated into neurons, iPSCs facilitate the assessment of drug responsiveness and the discovery of novel therapeutics. Moreover, with the integration of genome editing technologies, these cells may contribute to the development of personalized cell-based therapies [Que et al., 2021]. Additionally, advances in 3D stem cell culture systems have enabled the generation of brain organoids, which provide physiologically relevant in vitro platforms for studying disease mechanisms and testing therapeutic interventions in a human-like neural environment [Jang et al., 2014].

This study utilized microelectrode array (MEA) technology to perform electrophysiological analyses, assessing both neuronal network activity and responses to pharmacological treatment. Previous research using single-cell patch-clamp recordings revealed increased action potential firing in neurons carrying the SCN2A-L1342P variant. However, whether such intrinsic hyperexcitability translates into heightened activity at the network level has remained uncertain. MEA technology provides a high-throughput, non-invasive platform for extracellular recordings, enabling the monitoring of population-level neuronal dynamics under standardized culture conditions. This approach offers a physiologically relevant framework for evaluating network excitability [Que et al., 2021]. The use of MEA in combination with patient-derived iPSCs enables direct modeling of individual-specific neuronal phenotypes and interindividual variability. In the present study, network-level analyses were performed under conditions optimized to recapitulate the cortical microenvironment, thereby enhancing the translational relevance and potential in vivo applicability of the findings.

MEA analysis demonstrated that neurons derived from the corrected isogenic line exhibited minimal spontaneous activity, substantially reduced bursting behavior, restricted spatial activation, and limited network synchrony compared to neurons carrying the SCN8A c.4871T>G mutation. In contrast, SCN8A-mutant neurons displayed marked hyperexcitability, characterized by frequent and widespread network bursts. These findings indicate that precise correction of the SCN8A mutation restores normal neuronal function, reduces hyperexcitability, and suppresses aberrant network-level synchronization. This highlights the therapeutic relevance of gene correction strategies for SCN8A-related epileptic encephalopathies and provides a robust in vitro platform for mechanistic investigations.

In the central nervous system, voltage-gated sodium channels inactivate through two distinct processes—fast and slow inactivation—each differing in their kinetics and molecular

underpinnings. Fast inactivation occurs within milliseconds following depolarization and is mediated by a cytoplasmic linker between domains III and IV of the channel, which acts as a rapid gating mechanism to reduce sodium conductance. During prolonged depolarization or repetitive stimulation, channels transition into a slow inactivation state, involving structural rearrangements in the selectivity filter and S6 pore-lining segments. This conformational shift results in a progressive decline in sodium conductance over seconds to minutes, with recovery upon repolarization occurring slowly [William et al., 2020]. In this study, we examined the differential pharmacological effects of phenytoin and lacosamide, two ASMs that target distinct sodium channel inactivation pathways. Phenytoin enhances fast inactivation, while lacosamide selectively facilitates slow inactivation, thereby stabilizing the non-conducting state of the channel. In SCN8A-mutant neurons, phenytoin significantly reduced overall firing rates; however, parameters crucial for seizure generation—such as network burst duration and synchrony—were significantly decreased only at the highest concentration. Lacosamide also reduced firing rates and demonstrated a broader dose-dependent suppression of burst duration compared to phenytoin, but showed no significant impact on synchrony index. In contrast, both drugs significantly suppressed network burst metrics in corrected neurons, including parameters that were unresponsive to drug treatment in the mutant line. These observations suggest that SCN8A-mutant neurons exhibit a drug-resistant phenotype, particularly in network-level excitability. Phenytoin did not significantly alter firing rates in corrected neurons, suggesting that it may have a milder effect on baseline neuronal activity compared to lacosamide. The two drugs also displayed distinct effects across specific network parameters: phenytoin failed to reduce burst frequency, while lacosamide significantly attenuated it. Lacosamide further demonstrated a consistent reduction in burst duration over a wider range of concentrations. In contrast,

phenytoin selectively decreased synchrony index, but only at high doses, whereas lacosamide did not elicit significant changes in synchrony.

Taken together, these complementary effects support the potential benefit of dual therapy, offering a mechanistic rationale for combination treatment approaches in drug-resistant epilepsy. This is particularly relevant given that phenytoin and lacosamide target distinct aspects of network excitability. Previous studies using hiPSC-derived neurons have demonstrated that compounds such as riluzole and phenytoin can effectively modulate specific SCN8A variants, reducing pathological bursting activity in vitro [Tidball et al., 2020]. The hiPSC-derived neuronal model is well-suited for high-throughput pharmacological screening, enabling efficient assessment of candidate compounds and emphasizing its translational relevance. These in vitro platforms facilitate the discovery of novel therapeutics and serve as a foundation for precision medicine approaches, providing insight that may guide individualized treatment strategies in clinical contexts.

In this study, we generated iPSCs from a patient harboring a novel SCN8A mutation and applied precise gene editing to correct the mutation. The corrected iPSCs were successfully differentiated into both GABAergic and glutamatergic neurons. We confirmed functional neuronal network activity under conditions simulating the physiological cortical environment and observed a significant reduction in network excitability following gene correction. Furthermore, we characterized the drug resistance conferred by the mutation and investigated differential responses to sodium channel inhibitors with distinct mechanisms of action. These findings suggest that combination therapy may be an effective strategy for managing this specific SCN8A mutation. Future investigations will focus on evaluating the efficacy of dual treatment with phenytoin and lacosamide using patient-specific neurons. Additionally, we aim to identify novel pharmacological agents with therapeutic potential for SCN8A-associated epileptic encephalopathies.

5. Conclusion

In this study, we explored the functional consequences of newly identified SCN8A variants using neurons differentiated from human iPSCs. Our analyses revealed pronounced network-level hyperexcitability and hypersynchrony. We successfully established a patient-specific in vitro platform for pharmacological testing, enabling detailed investigation of mutation-specific responses. These findings contribute to the understanding of the cellular mechanisms underlying seizure activity caused by novel SCN8A mutations and represent a significant step toward the development of personalized therapeutic strategies for patients harboring pathogenic variants in SCN8A.

Looking ahead, we aim to identify new therapeutic compounds with efficacy against SCN8A-related epileptic encephalopathies. Additionally, comparative studies utilizing iPSCs derived from patients with SCN8A mutations of differing clinical severity will be essential for delineating the neurobiological and electrophysiological mechanisms underlying phenotypic variability in this disorder.

REFERENCES

Catterall WA, Lenaeus KJ, Gamal El-Din TM. Structure and Pharmacology of Voltage-Gated Sodium and Calcium Channels. (2020). Annu. Rev. Pharmacol Toxicol, 60, 133–54. doi.org/10.1146/annurev-pharmtox-010818-021757

Du X, Parent JM. (2015). Using Patient-Derived Induced Pluripotent Stem Cells to Model and Treat Epilepsies. Curr Neurol Neurosci Rep, 15, 71. doi. 10.1007/s11910-015-0588-3

Ellis CA, Petrovski S, Berkovic SF. (2020). Epilepsy genetics: clinical impacts and biological insights. Lancet Neurol, 19, 93–100. doi: org/10.1016/S1474-4422(19)30269-8

Hebbar M, Mefford HV. (2020). Recent advances in epilepsy genomics and genetic testing. F1000Res, 12:9:F1000 Faculty Rev-185. doi: 10.12688/f1000research.21366.1. eCollection 2020.

Jang J, Quan Z, Yum YJ, Song HS, Paek S, Kang HC. (2014). Induced pluripotent stem cells for modeling of pediatric neurological disorders. Biotechnol J, 9, :871-81. doi: 10.1002/biot.201400010.

Meisler MH, Helman G, Hammer MF, Fureman BE5, Gaillard WD, Goldin AL, Hirose S, Ishii A, Kroner BL, Lossin C, Mefford HC, Parent JM, Patel M, Schreiber J, Stewart R, Whittemore V, Wilcox K, Wagnon JL, Pearl PL, Vanderver A, Scheffer IE. (2016). *SCN8A* encephalopathy: Research progress and prospects. Epilepsia, 57, 1027–1035. doi:10.1111/epi.13422.

Meisler MH, Hill SF, Yu W. (2021). Sodium channelopathies in neurodevelopmental disorders. Nat Rev Neurosci, 22, 152–166. doi: 10.1038/s41583-020-00418-4

Musto E, Gardella E, Møller RS. (2020). Recent advances in treatment of epilepsy-related sodium channelopathies. Eur J Paediatr Neurol, 24, 123–128. doi: 10.1016/j.ejpn.2019.12.009

Que Z, Olivero-Acosta MI, Zhang J, Eaton M, Tukker AM, Chen X, Wu J, Xie J, Xiao T, Wettschurack K, Yunis L, Shafer JM, Schaber JA, Rochet JC, Bowman AB, Yuan C, Huang X, Hu CD, Trader DJ, Skarnes WC, Yang Y. (2021). Hyperexcitability and Pharmacological Responsiveness of Cortical Neurons Derived from Human iPSCs Carrying Epilepsy-Associated Sodium Channel Nav1.2-L1342P Genetic Variant. J Neurosci, 41, 10194-10208. doi: 10.1523/JNEUROSCI.0564-21.2021

Sa S, Nguyen DT, Pegan JD, Khine M, McCloskey KE. Round-bottomed Honeycomb Microwells: Embryoid body shape correlates with stem cell fate. (2012). J. Dev. Biol. Tissue Eng, 4, 12-22. doi.org/10.5897/JDBTE11.025

Scheffer IE, Berkovic S, Capovilla G, Connolly MB, French J, Guilhoto L, Hirsch E, Jain S, Mathern GW, Moshe SL, Nordli DR, Perucca E, Tomson T, Wiebe S, Zhang YH, Zuberi SM. ILAE classification of the epilepsies: Position paper of the ILAE Commission for Classification and Terminology. (2017). Epilepsia, 58, 512–521. doi: 10.1111/epi.13709

Sole L, Wagnon JL, Tamkun MM. (2020). Functional analysis of three Nav1.6 mutations causing early infantile epileptic encephalopathy. BBA - Molecular Basis of Disease, 1866.165959. doi: 10.1016/j.bbadis.2020.165959

Tidball AM,Lopez-Santiago LF, Yuan Y, Glenn TW, Margolis JL, Walker JC, Kilbane EG, Miller CA, Bebin EM, Perry MS, Isom LL, Parent JM. (2020). Variant-specific changes in persistent or resurgent sodium current in SCN8A-related epilepsy patient-derived neurons. BRAIN, 143, 3025–3040. doi:10.1093/brain/awaa247

Trimmer JS, Rhodes KJ. (2004). Localization of voltage-gated ion channels in mammalian brain. Annu Rev Physiol, 66, 477–519. doi: 10.1146/annurev.physiol.66.032102.113328

William ACl, Michael JL, Tamer MGED. (2020). Structure and Pharmacology of Voltage-Gated Sodium and Calcium Channels. Annu Rev Pharmacol Toxicol, 60, 133-154.

doi.org/10.1146/annurev-pharmtox-010818-021757

Abstract in Korean

최신 CRISPR/CAS9 시스템을 이용한 SCN8A 관련 발달 및 뇌전증성 뇌병증 환자 유래 유도만능줄기세포의 유전자 치료

배경:

SCN8A 유전자 변이는 발달 및 뇌전증성 뇌병증(developmental and epileptic encephalopathy)의 주요 원인 중 하나로, 조기에 발병하는 경련발작과 신경발달 장애를 일으킨다. 그러나 아직 효과적인 질병 모델과 치료는 제한적이다.

목적:

본 연구는 SCN8A 관련 뇌전증을 환자 유래 유도만능줄기세포(induced pluripotent stem cells, iPSCs)를 이용하여 모델화하고, 프라임 편집(prime editing)을 통한 유전자 교정을 수행한 후, 돌연변이 세포와 교정된 세포 간의 신경생리학적 및 약리학적 반응을 비교하였다.

방법:

SCN8A c.4871T>G (p.Ile1624Ser) 변이를 보유한 환자로부터 iPSCs를 제작하고, 프라임 편집(prime editing) 기법을 이용하여 유전적 교정을 수행하였다. ASCL1, DLX2, NGN2 전사인자를 렌티바이러스를 통해 발현시켜 뉴런으로 분화시킨 뒤, 다중전극배열(multielectrode array) 분석을 통해 신경 네트워크 활동을 평가하였고, phenytoin 및 lacosamide의 약리학적 효과를 분석하였다.

결과:

환자 유래 뉴런은 과흥분성, 빈번한 돌발(burst), 과동기화를 나타낸 반면, 교정된 뉴런은 정상적인 전기생리학적 활동을 보였다. 프라임 편집은 네트워크 기능을 효과적으로 복구하였다. Phenytoin과 lacosamide의 회로망 돌발 지수(network burst index)에서 효과는 교정된 세포에서 더 뚜렷하게 나타나서 환자의 약물 저항성 경향을 확인하였다. 또한 두 약물에 대해 서로 보완된 효과가 관찰되어 복합 치료 전략의 가능성을 보여주었다.

결론:

환자 유래 iPSCs 기반 뉴런 모델은 SCN8A 관련 뇌전증을 잘 재현할 수 있었다.

유전자 교정을 통해 병적 신경활동이 정상화되었으며, 환자 기반의 세포로 약물 반응을 확인할 수 있어 정밀 유전자 편집과 개인 맞춤형 약물 치료 전략의 가능성을 제시하고자 한다.

핵심되는 말: SCN8A; 유도만능줄기세포; 프라임 편집; 뇌전증; 뉴런 과흥분성; 다중 전극배열